6-1-1985

Report on High Intensity Solar Cells. Period Covered: June 1, 1983 to November 4, 1984

R. J. Schwartz
Purdue University

J. L. Gray
Purdue University

M. S. Lundstrom
Purdue University

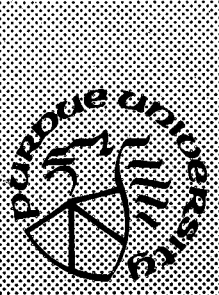

Report on High Intensity Solar Cells

Period Covered:
June 1, 1983 to
November 4, 1984

R. J. Schwartz
J. L. Gray
M. S. Lundstrom

TR-EE 85-11
June 1985

School of Electrical Engineering
Purdue University
West Lafayette, Indiana 47907

REPORT ON
HIGH INTENSITY SOLAR CELLS

Period covered: June 1, 1983 to November 4, 1984

R. J. Schwartz

J. L. Gray

M. S. Lundstrom

School of Electrical Engineering

Purdue University

West Lafayette, Indiana 47907

TR-EE 85-11

June 1985

TABLE OF CONTENTS

1. INTRODUCTION

1.1. Program Objectives

The purpose of this program is to provide general analytic support to Sandia National Laboratory's effort to develop high efficiency, high concentration solar cells. This support has taken the following forms:

1) Implementation of the two-dimensional silicon code on Purdue's Cyber 205.
2) The release of both the one- and two-dimensional silicon codes to Sandia National Laboratory.
3) Continued enhancement of the codes and updating of the physical models used by the codes.
4) Use of the two-dimensional code to investigate the performance and design of high concentration solar cells.

1.2. Period Covered by this Report

This report covers work performed between June 1,1983 and November 4, 1984.

1.3. Summary of Accomplishments

In addition to providing analytic support to Sandia, support has also been provided to various agencies and institutions. These include the University of Delaware, Cleveland State University, NASA-Lewis, ASEC, ARCO Solar, Westinghouse, Spire Corporation, the University of Arizona, the National Bureau of Standards, MIT Lincoln Laboratory, Jet Propulsion Laboratory, SERI, MACOM, SUNY, and Washington University.

The two-dimensional silicon solar cell simulation code, SCAP2D, has been implemented on Purdue's Cyber 205. Although the previous version of this code used iterative techniques to solve the linearized system of equations arising from the numerical solution of the semiconductor equations [1], the speed and virtual memory capabilities of the Cyber 205 have allowed a direct solution of these equations. This has made the code faster and much more reliable. A typical current-voltage

characteristic takes about 5 minutes of CPU time on the Cyber 205. The previous version of SCAP2D, which ran on a CDC6600, needed as much as 3 hours of CPU time to generate a current-voltage characteristic. In addition, modifications have been made in SCAP2D to include the effects of carrier-carrier scattering on mobility and allow for non-ideally ohmic electrical contacts. These modifications are detailed in Chapter 2.

Calculations were made to determine the theoretical limit of efficiency of silicon concentrator cells. These calculations indicated that properly designed and fabricated cells may approach efficiencies of 30% at 100 suns. A complete description of these calculations is given in Chapter 3.

Several papers were published during this report period. Copies of these papers appear in the Appendices.

Appendix A contains a paper which appeared in *Solar Cells* [4]. In this paper, the factors which limit the performance of high concentration silicon solar cells are reviewed. The design of a conventional high concentration cell is discussed, and the present state of the art is presented. The many unconventional cell designs which have been proposed to overcome the limitations of the conventional design are reviewed and compared, and the present status of unconventional cells is presented.

The two-dimensional simulation code, SCAP2D, was used to investigate the effects of radiation damage on the performance of the EMVJ and grating solar cells designed for space applications. This paper [5], which is reproduced in Appendix B, was presented at the Space Photovoltaics Research and Technology Conference at NASA-Lewis in October 1983.

The phenomena which limit the performance of concentrator cells were examined in a paper which appeared in *Solar Cells* [6]. These phenomena include contact grid shadowing, reflective losses, series resistance, and recombination mechanisms. These are examined individually to determine whether and how their effects on cell performance can be reduced or eliminated. It is concluded that a significant improvement in cell efficiency may yet be realized. A copy of this paper appears in Appendix C.

Appendix D contains a paper which was presented at the Seventeenth IEEE Photovoltaics Specialists Conference [7]. In it, SCAP2D was used to examine cell geometries designed for high efficiency. These include the conventional, IBC, EMVJ, and grating cells. It is concluded that recombination at ohmic metal contacts is the major factor limiting cell performance and that novel contact designs could increase the efficiencies of concentrator cells dramatically.

A paper, which appears in Appendix E, describing the current status of the one- and two-dimensional modeling codes was presented at the High-Efficiency Chrystaline Silicon Solar Cell Research Forum in Phoenix, Arizona in July 1984 [8]. In it, the capabilities of the codes were described and the occasions when a two-dimensional model is required were discussed. The application of the models to design, analysis, and prediction were presented along with a discussion of problem areas for solar cell modeling.

2. SCAP2D MODIFICATIONS

2.1. Introduction

Purdue's Cyber 205 became available for limited use during the spring of 1983. As was recommended in a previous report [1], it was decided to convert SCAP2D to run on this machine. Implementation on this machine has several advantages. The virtual memory capability of the Cyber 205 and its faster CPU allow a direct solution of the Jacobi matrix equation to be performed. This has completely eliminated problems with convergence for certain device geometries when iterative methods were used. As a result, this makes SCAP2D much less operator dependent and makes it as easy and straight-forward to use as SCAP1D. In addition, since the Cyber has vector processing capabilities, vectorization of the linear equation routines increase the speed even more. A typical current-voltage (I-V) characteristic takes about 5 minutes of CPU time on the Cyber 205.

Since implementation of SCAP2D on the Cyber 205 serves only to improve the speed with which simulations are obtained, the reader is referred to [1,2,3] for the details of the problem formulation. The discussion here will be limited to modifications made during the report period to the physical models used by SCAP2D.

A two-dimensional computer model of solar cells is necessary because most solar cell geometries exhibit two-dimensional behavior under high illumination (high injection) conditions. Then, under high injection conditions, the effects of carrier-carrier scattering on mobility become significant and must be included in the computer model. The model we use for carrier-carrier scattering is described in the next section.

It is apparent that the fabrication of contacts that act as good minority carrier mirrors while remaining ohmic to majority carriers is a desirable objective. SCAP2D has been modified to allow the effects of the electrical contact on device performance to be investigated. This modification is explained in section 2.3.

2.2. Carrier-Carrier Scattering and Mobility

SCAP2D has the capability of using two different empirical models for the mobility in doped single crystal silicon. The models are a Caughey-Thomas formula

[9] with updated constants [10,11] and a similar model proposed by Arora, et.al. [12]. Dorkel and Leturcq [13] have proposed a mobility model which also includes the effects of carrier-carrier scattering. Unfortunately, their expression for the component of mobility due to impurity scattering is inaccurate for doping levels above 10^{19} cm^{-3}, making direct usage of their empirical expressions impossible since the emitter and collector (high-low junction) of solar cells are often doped in excess of 10^{20} cm^{-3}.

Carrier-carrier scattering has been incorporated by assuming that the lattice-impurity scattering components of the mobility (as given by the Caughey-Thomas or Arora models) and the carrier-carrier scattering component combine as follows.

$$\frac{1}{\mu_n} = \frac{1}{\mu_{li,n}} + \frac{1}{\mu_{ccs}} \tag{2-1}$$

and

$$\frac{1}{\mu_p} = \frac{1}{\mu_{li,p}} + \frac{1}{\mu_{ccs}} \tag{2-2}$$

The subscript "li" refers to the lattice-impurity component and the subscript "ccs" refers to the carrier-carrier scattering component.

The carrier-carrier scattering component is given by [13]

$$\mu_{ccs} = \frac{2\times10^7\, T^{3/2}}{(pn)^{1/2}}\left[\ln\left(1 + 8.28\times10^8\, T^2 (pn)^{-1/3}\right)\right]^{-1} \tag{2-3}$$

It should be noted that although the mobility is now injection level dependent and therefore modifies the Jacobi matrix, these modifications are ignored and the mobility is merely updated after each Newton iteration. For the cases that have been encountered thus far, this has no effect on the rate of convergence of the Newton iteration.

2.3. Modeling of Electrical Contacts

At ideally ohmic contacts, the carrier concentrations are assumed to be at their equilibrium values. Thus, in effect, the contacts are treated as surfaces with an infinite surface recombination velocity. To allow for the possibility of non-ideal ohmic contacts, SCAP2D has been modified so that the contacts can be modeled as surfaces with finite surface recombination velocities.

For an electrical contact to a p-type semiconductor, the normal components of the hole and electron currents flowing into the contact are modeled as follows.

$$J_p = qS_{pp}\Delta p \tag{2-4}$$

$$J_n = -qS_{np}\Delta n \tag{2-5}$$

S_{pp} is the effective surface recombination velocity for holes at a p-type contact, S_{np} is the effective surface recombination velocity for electrons at a p-type contact, and Δp and Δn are the excess hole and electron concentrations at the contact. Contacts to n-type semiconductors are modeled similarly.

Typically, the majority carrier surface recombination velocity is taken to be the thermal velocity, while the minority carrier surface recombination velocity is selected to match the assumed minority carrier reflecting properties of the electrical contact.

3. ESTIMATION OF EFFICIENCY LIMITS

3.1. Introduction

The design of high efficiency solar cells requires an understanding of the interaction of the recombination mechanisms affecting cell efficiency. These recombination mechanisms have been examined in a paper which has been reproduced in Appendix A [4]. It was concluded that all sources of recombination can probably be reduced to negligible levels by proper cell design and fabrication, except for recombination in the base region of the solar cell. Given this assumption, it is possible to write a current-voltage expression for this ideal device in terms of the cell's thickness and base doping. Given a solar spectrum and concentration level, the efficiency of this ideal cell for a given thickness and base doping can be computed. These calculations were presented in a paper which is reproduced in Appendix D [7]. The analysis is repeated here, except that Auger recombination is included and a higher base lifetime is assumed.

3.2. Estimation of Efficiency Limits

If the only source of recombination occurs in the base of the solar cell, and if the base width is smaller than a diffusion length, then the cell current can be approximated as follows:

$$J(V_j,W,N) = q\int_0^W G(x)dx - q\int_0^W R(x)dx\,, \qquad (3\text{-}1)$$

where V_j is the applied voltage across the pn junction, W is the base thickness, N is the base doping, and G(x) is the optical generation rate associated with the incident spectrum and the assumed optical properties of the cell.

The cell voltage is the sum of three terms: V_j, the pn junction voltage; V_{hl}, the applied voltage across the high-low junction; and V_b, the ohmic drop across the base.

$$V_t(V_j,W,N) = V_j + V_{hl}(V_j,N) - V_b(V_j,W,N) \qquad (3\text{-}2)$$

Since under our assumptions the carrier concentrations in the base are independent of position, there are no Dember potentials.

Assuming recombination in the base is controlled by a SHR midgap trap and band-band Auger recombination, the recombination current is just

$$q\int_0^W R(x)dx = qW(pn-n_{ie}^2)\left[A_n n + A_p p + \frac{1}{\tau(n+p+2n_{ie})}\right] \tag{3-3}$$

where $A_n = 2.8\times10^{-31}$ cm^6/s and $A_p = 9.9\times10^{-32}$ cm^6/s are the Auger recombination coefficients [14] and $\tau = \tau_p = \tau_n$ has the following empirical doping dependence [15].

$$\tau = \frac{1000\,\mu\text{sec}}{1+\frac{N}{7.1\times10^{15}}} \tag{3-4}$$

This assumes that the best attainable lifetime in low doped silicon is about 1 ms. An empirical expression for the effective intrinsic carrier concentration, n_{ie}, suggested by Slotboom and DeGraaff [16] has been used. Although this formula is based on measurements of p-type silicon, it was assumed in these calculations that it is also valid for n-type material.

The excess carrier concentration in the base is easily computed in terms of the applied voltage across the pn junction, V_j. Since the excess carrier concentration is assumed to be uniform throughout the base, the excess carrier concentration can then be used to compute V_{hl}.

The ohmic drop across the base is computed from the following, where the mobility model of Leturcq, et. al. [13], which includes carrier-carrier scattering has been used.

$$V_b = \frac{JW}{qn\mu_n + qp\mu_p} \tag{3-5}$$

Solar cell efficiency contour plots are shown in Figures 3-1 to 3-5 for n-type bases at 1, 10, 100, 500, and 1000 AM1.5 suns, respectively. The spectrum intensity has been normalized so that 1 sun corresponds to 100 mA/cm^2. The short base assumption breaks down for the region above and to the right of the heavy line, so the calculation is not valid there, although it still represents an upper limit.

The solar cell characteristics at the peak efficiencies are tabulated in Tables 3-1. It should be emphasized that these are only upper limits on device performance. Their main value is in demonstrating that considerable improvement may yet be attainable for single crystal solar cells. In addition, they give starting points for the base thickness and doping when using the simulation codes to design high efficiency solar cells.

Table 3-1.
Theoretical Performance Limits

	AM1.5 suns					
parameter	1	1	10	100	500	1000
V_{OC} (mV)	702	784	814	849	883	900
J_{SC} (A/cm^2)	.0416	.0386	.405	4.13	20.38	40.1
FF	.814	.823	.862	.883	.882	.883
η (%)	24.6	24.9	28.5	31.0	31.8	31.9
W (μm)	175	40	100	150	110	80
N (cm^{-3})	3×10^{16}	1×10^{11}	1×10^{11}	1×10^{11}	1×10^{11}	1×10^{11}

These results indicate that silicon solar cell efficiencies of nearly 25% at 1 sun and about 30% at several hundred suns may be possible. However, these high efficiencies can only be attained if recombination losses at the contacts, free surfaces, and in the heavily doped regions can be reduced to negligible levels. It is also apparent that these cells should, in general, be thin and lightly doped, although the restrictions are not severe. For example, at 100 suns, cells between 40 and 400 microns thick with base dopings of up to 1×10^{16} all have an efficiency of over 30%.

Much of the dependence of efficiency on cell thickness is due to the assumption of only a double pass of the incident light. If perfect light trapping properties are assumed, the trend is for the best cells to be as thin as possible. The dependence on base doping is roughly the same. For example, with the assumption of perfect light trapping, a 20 micron thick cell with a base doping of 1×10^{14} has a theoretical maximum efficiency of over 29% at 1 sun. This same cell at 500 suns has a maximum theoretical efficiency of nearly 36%.

3.3. Summary

Very high theoretical efficiencies are predicted for single crystal silicon solar cells. These predictions indicate that significant improvements may yet be possible for silicon cells. In order to achieve these high efficiencies, all recombination losses

must be minimized *simultaneously*. These include recombination at the contacts, at the free surfaces, in the heavily doped regions and in the base. If these can be properly controlled, then fabrication of cells with efficiencies approaching these high limits is possible.

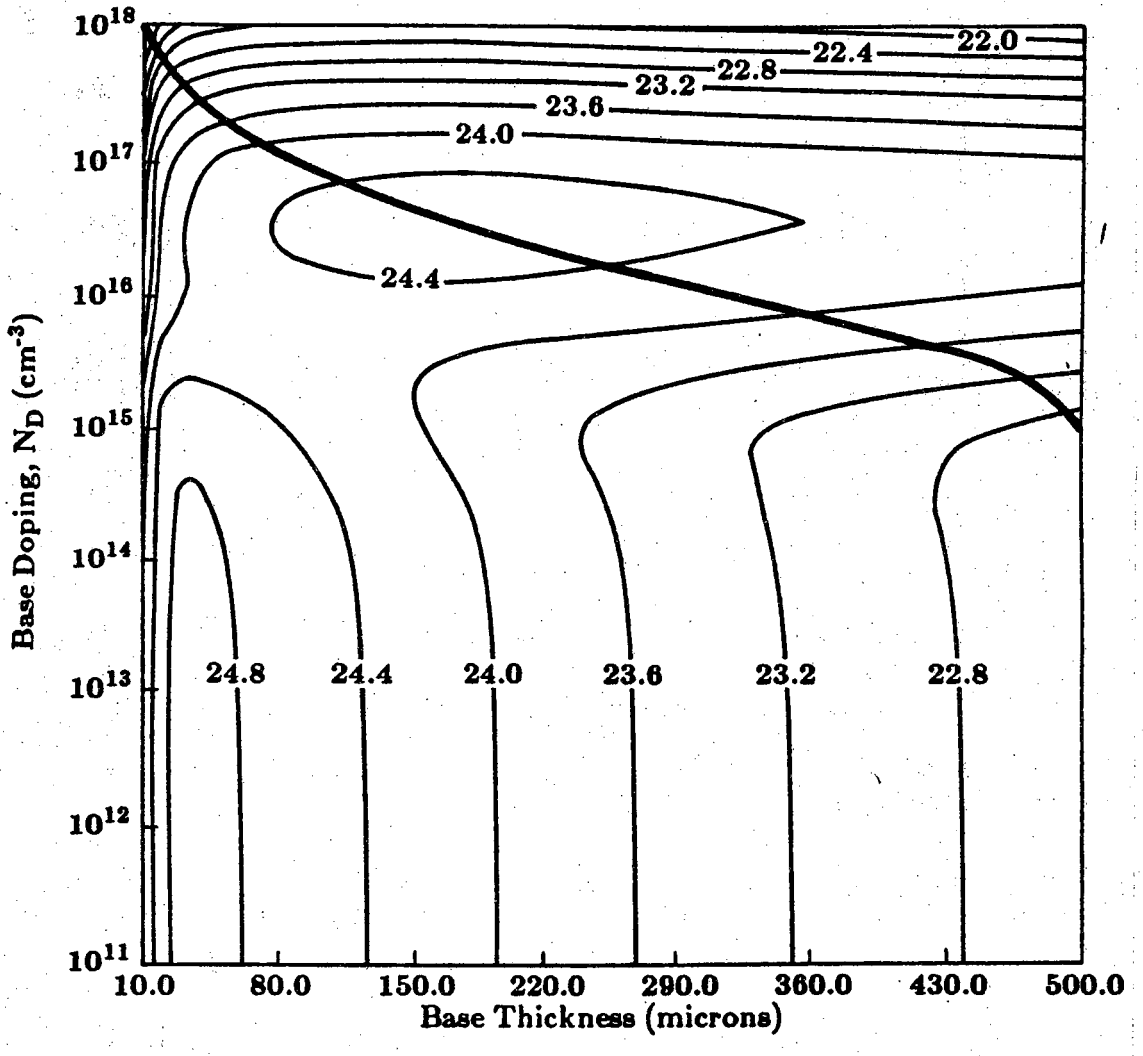

Figure 3-1
Contour Plot of Efficiency at 1 AM1 Sun.

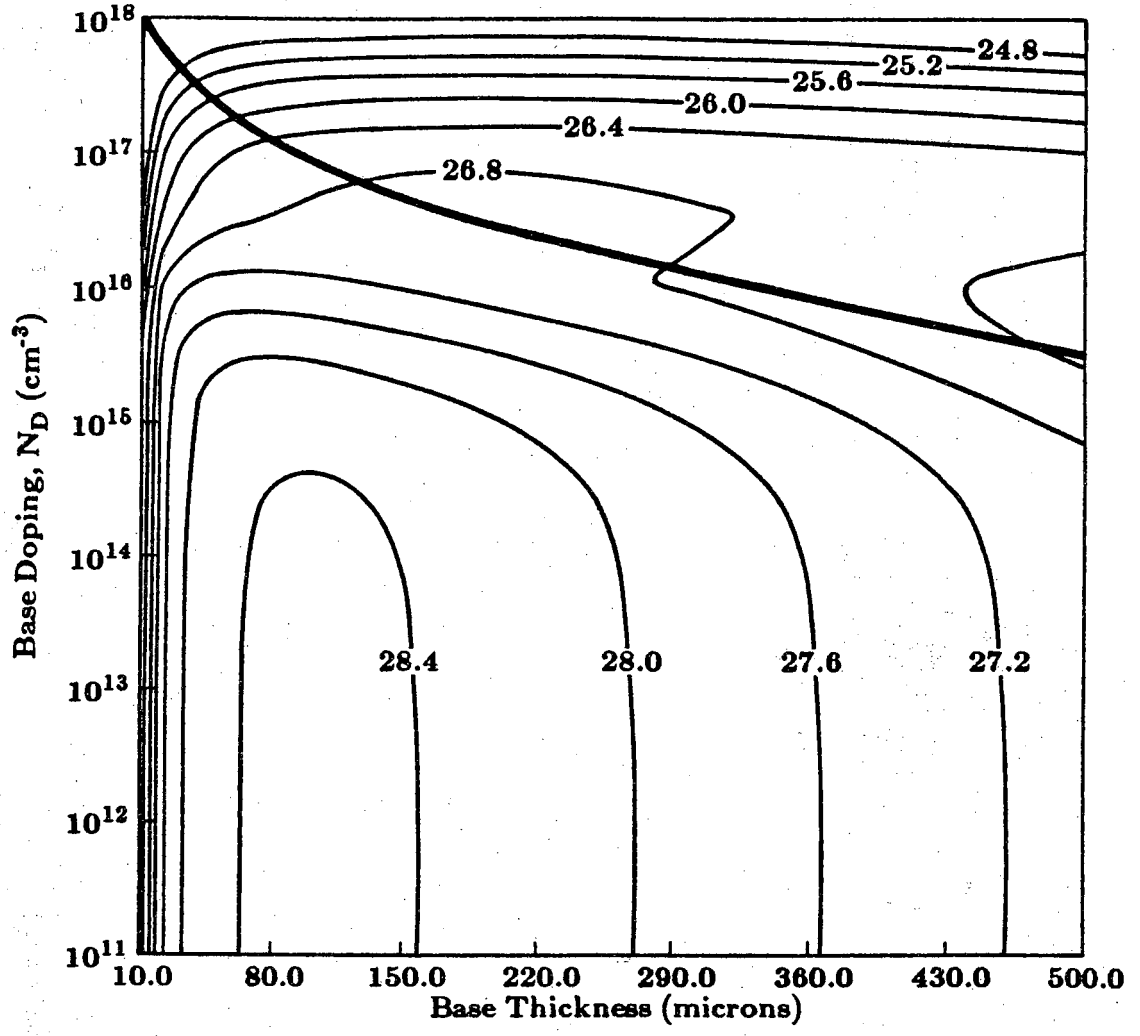

Figure 3-2
Contour Plot of Efficiency at 10 AM1 Suns.

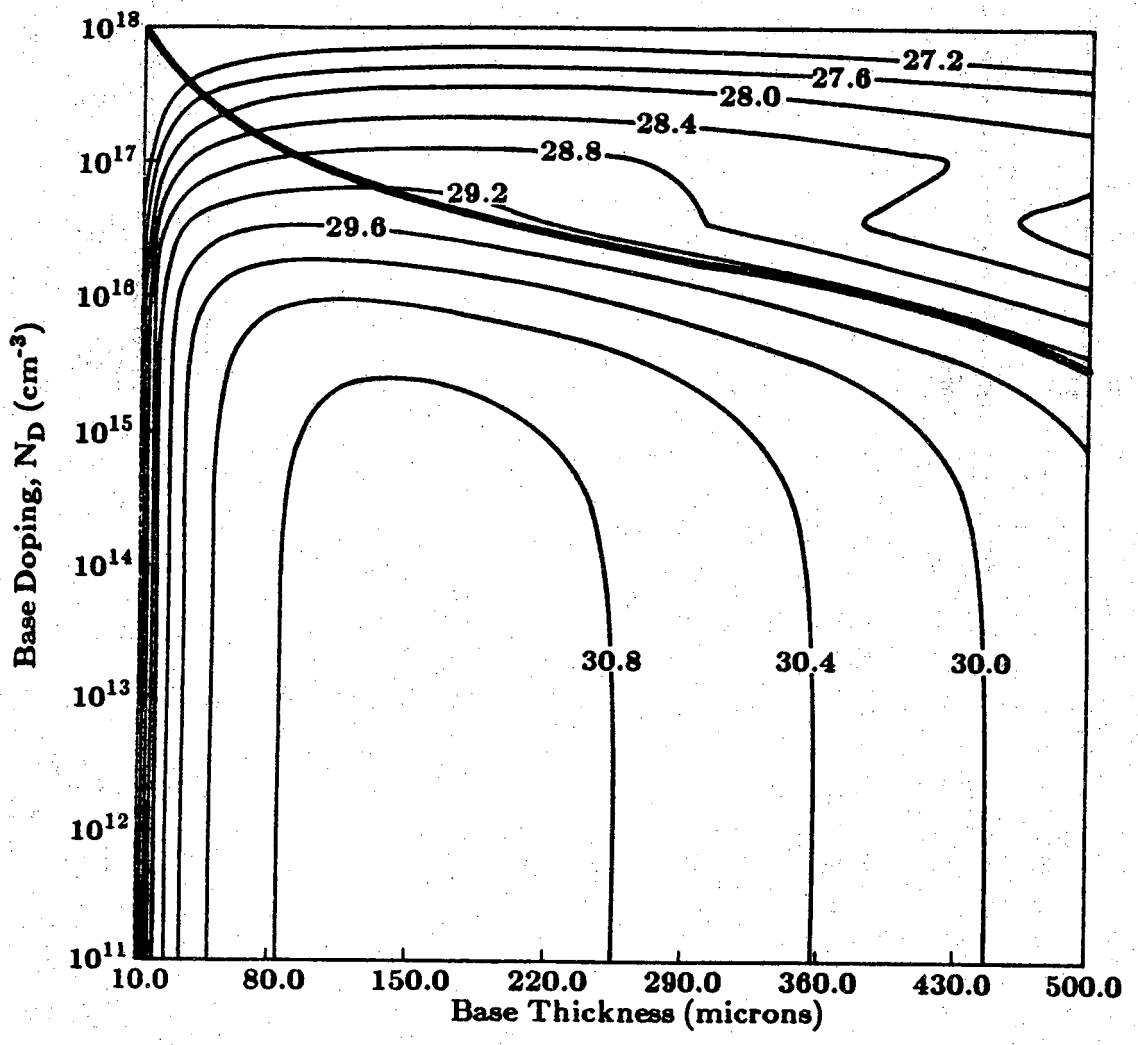

Figure 3-3
Contour Plot of Efficiency at 100 AM1 Suns.

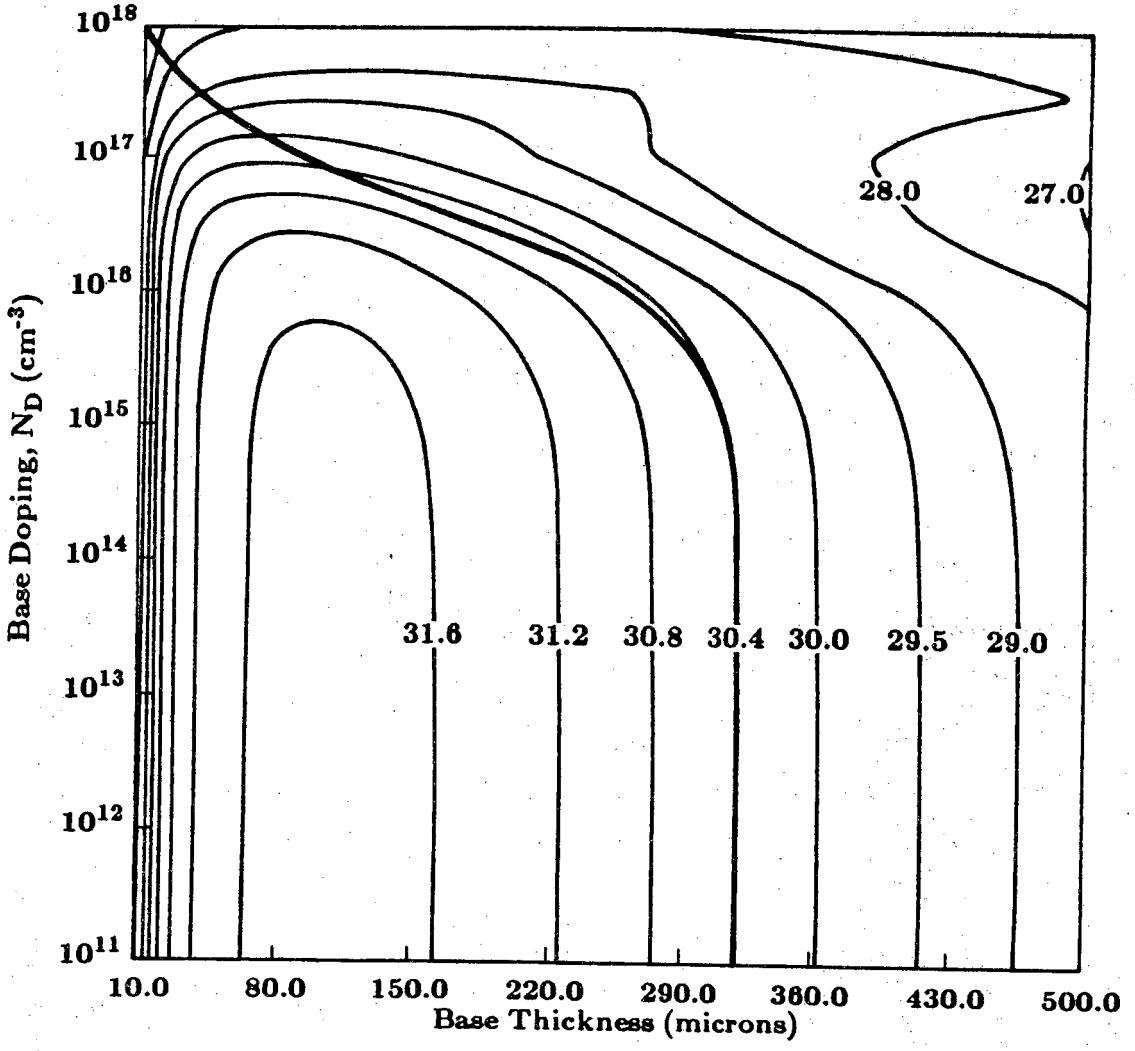

Figure 3-4

Contour Plot of Efficiency at 500 AM1 Suns.

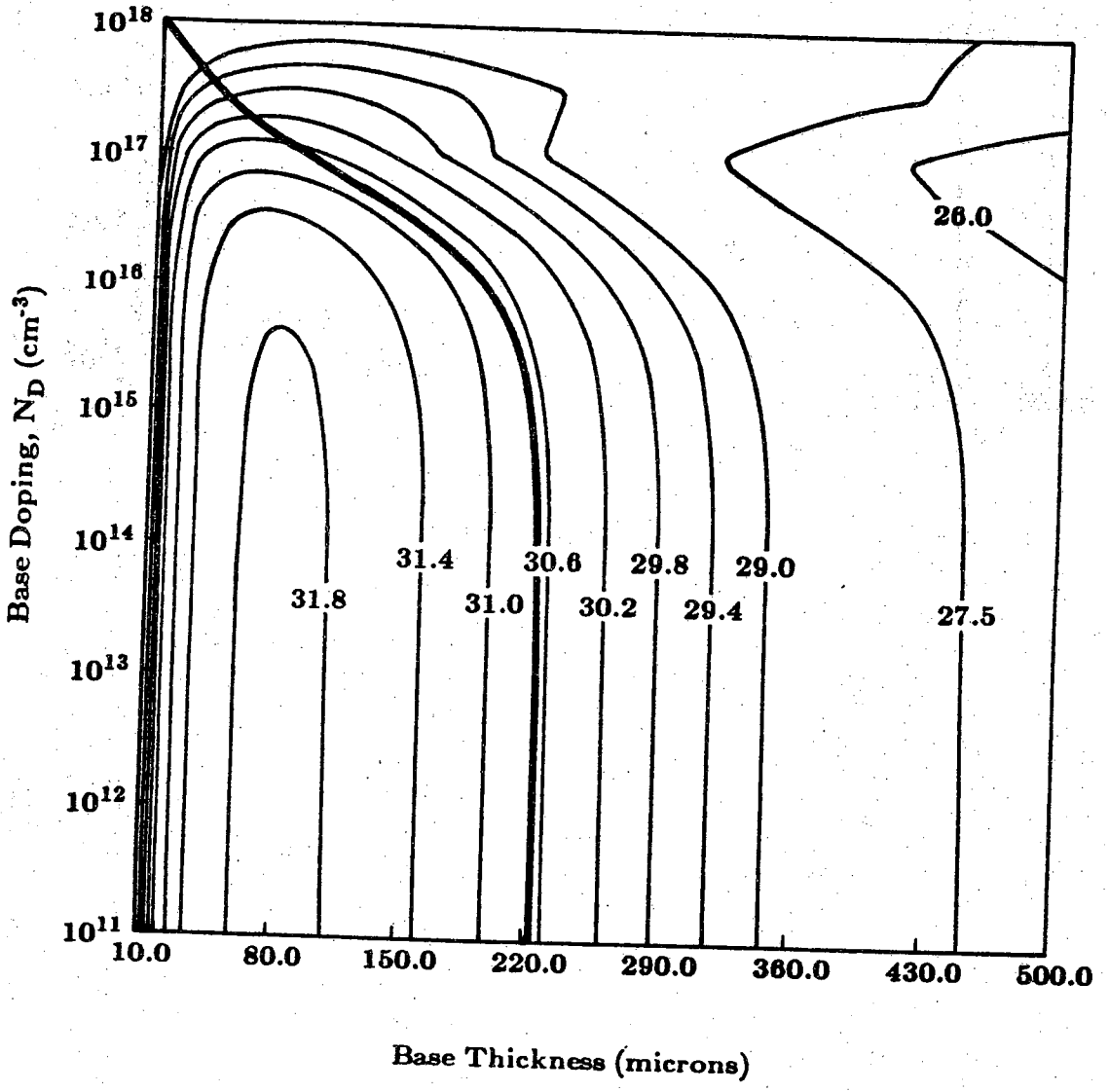

Figure 3-5
Contour Plot of Efficiency at 1000 AM1 Suns.

LIST OF REFERENCES

[1] R.J. Schwartz, J.L. Gray, and M.S. Lundstrom, "Report on High Intensity Solar Cells," TR-EE 83-21, Purdue University, West Lafayette, IN, February, 1983.

[2] R.J. Schwartz, M.S. Lundstrom, and J.L. Gray, "Annual Report on High Intensity Solar Cells," TR-EE 82-5, Purdue University, West Lafayette, IN, January, 1981.

[3] J.L. Gray, "Two-Dimensional Modeling of Silicon Solar Cells," TR-EE 82-12, Purdue University, West Lafayette, IN, August, 1982.

[4] R.J. Schwartz, "Review of Silicon Solar Cells for High Concentrations", Solar Cells (6), pp. 17-38, 1982.

[5] Two-Dimensional Simulation of the EMVJ and Grating Solar Cells Under AM0 Illumination," Space Photovoltaic Research and Technology Conference, NASA Lewis Research Center, Cleveland, Ohio, Oct. 18-20, 1983.

[6] R.J. Schwartz and J.L. Gray, "Performance Limits of Silicon Solar Cells," Solar Cells (12), pp. 197-203, 1984.

[7] J.L. Gray and R.J. Schwartz, "Two-Dimensional Computer Simulation of Single Crystal Silicon Solar Cells," Seventeenth Photovoltaic Specialists Conference, Kissimmee, Florida, May 1-4, 1984.

[8] R.J. Schwartz, J.L. Gray, and M.S. Lundstrom, "Current Status of One- and Two-Dimensional Numerical Models: Successes and Limitations," High Efficiency Crystalline Silicon Solar Cells Research Forum, Phoenix, Arizona, July 9-11, 1984.

[9] D.M. Caughey and R.E. Thomas, "Carrier Mobilities in Silicon Empirically Related to Doping and Field," Proc. IEEE, 55, pp.2192-2193, 1967.

[10] J.C. Plunkett, J.L. Stone, and A. Leu, "A Computer Program for Accurate and Repeatable Profile Analysis Using Anodization and Stripping of Silicon", Solid-State Electron., 20, pp. 447-453, 1977.

[11] G. Baccarani and P. Ostoja, "Electron Mobility Empirically Related to the Phosphorous Concentration in Silicon," Solid-State Electron., 18, pp. 579-580, 1975.

[12] N.D. Arora, J.R. Hauser, and D.J. Roulston, "Electron and Hole Mobilities in Silicon as a Function of Concentration and Temperature," IEEE Trans. Electron Devices, ED-29(2), pp. 292-295, Feb. 1982.

[13] J.M. Dorkel and Ph. Leturcq, "Carrier Mobilities in Silicon Semi-empirically Related to Temperature, Doping, and Injection Level," Solid-State Electron., 24(9), pp. 821-825, 1981.

[14] J. Dziewoir and W. Schmid, "Auger Coefficients for Highly Doped and Highly Excited Silicon," Appl. Phys. Lett., 31, pp. 346-348, 1977.

[15] J.G. Fossom, "Computer-Aided Numerical Analysis of Silicon Solar Cells," Solid-State Electron., 19, pp. 269-277, 1976.

[16] J.W. Slotboom and H.C. DeGraaff, "Measurements of Bandgap Narrowing in Si Bipolar Transistors," Solid-State Electron., 19, pp. 857-862, 1976.

APPENDIX A

This appendix contains a paper which appeared in *Solar Cells* [4].

Solar Cells, 6 (1982) 17 - 38

REVIEW OF SILICON SOLAR CELLS FOR HIGH CONCENTRATIONS

R. J. SCHWARTZ

Purdue University, School of Electrical Engineering, West Lafayette, IN 47907 (U.S.A.)

(Received July 30, 1981; accepted August 28, 1981)

Summary

The factors which limit the performance of high concentration silicon solar cells are reviewed. The design of a conventional high concentration cell is discussed, and the present state of the art is presented. The many unconventional cell designs which have been proposed to overcome the limitations of the conventional design are reviewed and compared. The present status of unconventional cells is presented.

1. Introduction

Ever since their invention in 1954, silicon solar cells have received a great deal of attention for applications in unconcentrated and low concentration systems. The relative abundance of silicon, the existence of a highly developed silicon technology and a high level of understanding of the properties of silicon together with a large indigenous production capability for silicon devices make silicon an attractive candidate for a solar cell material, even though other materials have band gaps which are more closely matched to the solar spectrum. In recent years, silicon has been shown to be an excellent choice for high concentration applications also. Recent reports show that silicon is capable of conversion efficiencies in excess of 20% [1] and has been operated at concentration ratios as high as 1000 [2].

Initial attempts to use silicon solar cells under concentrated sunlight met with only modest success [3 - 6]. As the insolation level was increased on cells which were designed to operate at 1 sun, the efficiency was found to increase, to peak and then to decrease rapidly to levels which were no longer useful. Even though these early experiments were of limited success, they served to identify some of the problems which are of major concern in the design of today's concentrator solar cells.

The purpose of this review is to discuss the theory of operation of a silicon solar cell at high intensities, the factors which limit the operation of these cells, the techniques which are employed to overcome these limits, the present state of the art and future expectations.

0379-6787/82/0000-0000/$02.75

18

Some of the limits on conversion efficiency, such as reflection, are equally important in 1 sun cells and concentrator cells, while other problems such as series resistance, which affect both 1 sun and high concentration cells, are greatly aggravated by operation at high concentration. Some design constraints, such as the cell area, are imposed as a result of systems considerations, while others, such as the thickness of the device, may be imposed by fabrication considerations. Still others, such as the depth of the junction, may be imposed by the properties of the material and the solar spectrum.

Many cell designs which promise improved high concentration operation have been proposed; however, the highest reported conversion efficiency has been obtained in a solar cell of conventional design [1]. The operation of a cell of conventional design will be reviewed, and then the many unconventional cell designs which have been put forward will be examined. The relative advantages and disadvantages of each of them and their relationships to each other will be discussed. Finally, the expected future performance of silicon solar cells in concentrator systems will be examined.

2. The one-dimensional intrinsic solar cell

For an ideal intrinsic device the relationship between the current and voltage is given by

$$J = J_{sc} - J_0\left\{\exp\left(\frac{qV}{nkT}\right) - 1\right\} \tag{1}$$

The open-circuit voltage is

$$V_{oc} = \frac{nkT}{q} \ln\left(\frac{J_{sc}}{J_0}\right) \tag{2}$$

and the conversion efficiency η is given by

$$\eta = V_{oc} I_{sc} \frac{FF}{P_{inc}} \tag{3}$$

where P_{inc} is the incident power density and FF the fill factor. Examination of these equations illustrates one of the benefits of using a solar cell in a concentrator. The short-circuit current density J_{sc} is proportional to the insolation. The open-circuit voltage V_{oc} is proportional to the natural logarithm of the light intensity. The fill factor FF is nearly independent of the illumination level (under ideal conditions it actually increases slightly). Thus, the cell operating efficiency increases as the illumination intensity increases. This increase in efficiency will continue as the illumination intensity increases until extrinsic effects become large enough to dominate the performance of the cell.

2.1. Open-circuit voltage V_{oc}

The term J_0 which occurs in the expression for the open-circuit voltage (eqn. (2)) is given by

$$J_0 = J_n + J_p \tag{4}$$

If, as is typically the case, the minority carrier diffusion lengths in the emitter and base are much larger than the thickness of these regions, and if we consider first the case where the surface recombination velocity is large,

$$J_p = q \Big/ \int_0^{W_n} \frac{N_D(x)\,dx}{n_{ie}^2(x) D_p(x)} \tag{5}$$

and

$$n_{ie}^2 = n_{io}^2 \exp\left(\frac{\Delta G}{kT}\right) \tag{6}$$

where ΔG is the effective band gap narrowing parameter which is required to account correctly for various "heavy doping effects" [7]. A similar expression holds for J_n.

In the simplest case of no heavy doping effects and constant doping, eqn. (4) reduces to

$$J_0 = \frac{q n_{io}^2 D_p}{N_D W_n} + \frac{q n_{io}^2 D_n}{N_A W_p} \tag{7}$$

and the open-circuit voltage would be expected to increase, for fixed values of illumination level and diffusion coefficient, as the doping density of the two sides of the junction is increased. This is not what has been observed [8, 9]. The value of V_{oc} was observed to reach a maximum with a base doping density in the vicinity of 10^{17} - 10^{18} cm^{-3}. This discrepancy has subsequently been explained by an increase in the minority carrier concentration in the heavily doped regions (above 10^{17} cm^{-3}). The origins of the increase in the minority carrier concentration have not yet been definitively explained but they appear to be due to a reduction in the energy band gap [10, 11] and possibly due to a change in the density of states [7]. Whatever the origins of the effect, it has been shown that eqn. (5) is correct, provided that the value of n_{ie} is correct.

If, as has been proposed [12], the band gap narrowing is due to free carriers, this effect may impose an upper limit on the illumination level at which solar cells may be operated since it is possible to have the free-carrier concentration exceed 10^{17} cm^{-3} when an illumination of above 100 suns is used. However, both the base and the emitter would probably be relatively heavily doped in any cell which is likely to be operated in this concentration range and would therefore already experience the effect. Heavy doping effects are present in the emitter of all conventional solar cells as a result of the need to dope the emitter heavily to reduce the emitter sheet resistance.

The effects of surface recombination on the open-circuit voltage have been considered in detail by Fossum *et al.* [13]. If the emitter is transparent to minority carriers, *i.e.* if carriers can move from the surface to the collecting junction without significant recombination, and the base recombination is small, the open-circuit voltage will be determined by the lowest attainable surface recombination velocity.

There are three distinct regions to be considered for surface recombination in a conventional solar cell: the region immediately under the metal grid, the remainder of the illuminated surface and the rear or unilluminated surface.

The region immediately under the grid is a region of very high surface recombination. Because of the very high surface recombination associated with ohmic contacts, the contact area must be kept to a minimum if the emitter is shallow. The rest of the illuminated surface is usually passivated with a thermal oxide to keep the surface recombination to a minimum.

The effects of using a textured etch, which exposes a (111) surface rather than the lower surface state density (100) surface, on the surface recombination velocity have not been reported for concentrator cells, although a good blue response has been demonstrated.

The surface recombination velocity of the rear surface is usually high because much of this surface is covered by an ohmic contact with its associated high recombination velocity. The back-surface field, discussed below, is used to reduce the detrimental effects of this contact.

The temperature dependence of the efficiency of the cell is of critical concern in a concentrator cell because high insolation levels can elevate the cell temperature well above ambient temperatures. Also, since in some systems it is advantageous to obtain process heat together with the generation of electrical energy, the dependence of the electrical conversion efficiency on the temperature of the cell is a critical design parameter and may form a severe limit on the use of silicon cells in such systems. The primary temperature dependence of η is due to the dependence of V_{oc} on temperature.

The temperature dependence of V_{oc} is determined by the explicit dependence of eqn. (2) on T and by the implicit dependence of J_0 on temperature. There is a small temperature dependence of J_0 on D through the mobility dependence on T, but the major dependence is through the dependence of n_{ie} on T. n_{ie} is strongly dependent on the band gap, which is in turn temperature dependent. The effects of degeneracy on n_{ie} are also temperature dependent.

Typical values of the temperature dependence of V_{oc} are in the range of 2 mV $°C^{-1}$. A reduction in the temperature dependence of V_{oc} at high insolation levels has been reported [2].

2.2. *Short-circuit current* I_{sc}

The magnitude of I_{sc} is dependent on the number of hole–electron pairs which are optically generated and subsequently collected by the p–n junc-

tion. The generation rate is determined by the incident solar intensity, the illuminated surface reflectance and the absorption coefficient.

It is possible to reduce the reflectance of the cell to a value of 2% over the useful solar spectral range through the use of a coated textured surface [14]. No special problems with antireflecting surfaces have been encountered as a result of their use on high concentration cells, although textured surfaces have not yet received wide usage on these cells.

Silicon is an indirect gap material and as a consequence has a relatively low absorption coefficient near the band edge compared with a direct gap material such as GaAs. The result of this is that the silicon cells need to be thicker than direct gap cells in order to utilize efficiently the portion of the solar spectrum near the band edge. Highly reflecting rear surfaces can increase the optical thickness by causing the photons to make multiple passes through the cell.

The collection efficiency of the cells depends on the solar spectral distribution, the diffusion lengths, the surface properties and the contact configuration and method. The spectral dependence of I_{sc} occurs because the diffusion lengths of the emitter and base regions may be different and the distribution of generated carriers is spectrally dependent.

Diffusion lengths are reduced in heavily doped regions because of reductions in lifetime and/or mobility [15]. The lifetime is dependent on doping level, processing procedures and free-carrier concentrations. The reduction in lifetime which occurs with increased doping results in a significant reduction in lifetime in the emitter and base of some concentrator cells. In those regions which are very heavily doped or have very high free-carrier concentrations, the lifetime can be dominated by Auger recombination and in the latter case the lifetime will be free-carrier dependent. Even in those cases where the recombination is dominated by Hall–Shockley–Read processes, the lifetime may be a function of the illumination level since the lifetime will increase as the cell passes from low to high injection conditions.

3. Extrinsic limitations on the conversion efficiency of silicon solar cells

Extrinsic effects act to reduce the performance of the cell. They are generally subject to reduction through proper design, although they may not be eliminated altogether because of various design compromises which must be made. In this section we discuss the various extrinsic losses and the techniques used to minimize them.

3.1. Series resistance

As the concentration ratio increases, the attendant increase in I_{sc} causes the detrimental effects of the series resistance of the cell to become progressively more important. The presence of series resistance effects will reduce the conversion efficiency in two ways. Some of the electrical power which is generated by the intrinsic device is dissipated as Joule heat in the resistive

regions. Also, the presence of the lateral resistive voltage drop in the emitter causes the junction potential to be a function of position. This, in turn, means that only a portion of the device can be operating at the maximum intrinsic power point. There are three major sources of series resistance effects in a conventional well-designed solar cell: the contact grid; the thin heavily doped surface region; the base of the device.

3.1.1. The contact grid

At a concentration ratio of 100, I_{sc} may exceed 3.0 A cm^{-2} and will be correspondingly higher for higher concentration ratios. Because of the extremely high current densities encountered at high concentration, the design of the contact grid on the illuminated surface of the cell becomes more and more critical as the concentration ratio increases. In order to minimize grid resistance, shadowing and sheet resistance simultaneously, the aspect ratio (height to width) of the individual grid lines must be maximized and the grid spacing optimized.

The result is that the grid design consists of a set of very thin high aspect ratio lines with close spacing. These requirements usually rule out the use of screened-on grid lines as is common in low intensity cells. Concentrator cell grids are usually fabricated using photolithographic and electroplating techniques [16 - 18].

3.1.2. Emitter sheet resistance

A reduction in the lateral series resistance of the emitter requires that the sheet resistance of the layer be minimized. This in turn calls for a thick layer and heavy doping. Making the diffused layer thick, *i.e.* placing the junction deep, will reduce the short wavelength response of the cell. Increasing the doping to minimize sheet resistance will increase recombination in the emitter, causing a decrease in the short-circuit current and a loss of blue response. These requirements can be eased somewhat through the use of a grid of very fine lines with close spacing. Increasing the doping to reduce the sheet resistance will reduce the open-circuit voltage as a result of the heavy doping effects discussed in Section 2.1.

Typical concentrator cell emitter regions are 0.35 μm deep with a surface concentration in the vicinity of $(1 - 2) \times 10^{20}$ atoms cm^{-2}.

3.1.3. Base resistance

For large operating currents the resistance of the base region can significantly affect the performance of the solar cell near its maximum power operating point. Even though the base of the cell may be in high injection conditions when operated near open circuit (and hence the base resistance may be significantly reduced from its value under low injection conditions) a portion of the base may fall to low injection conditions and hence have a high resistance when the cell is operated near its maximum power point. The result is that a large voltage drop may develop in the base, severely degrading the fill factor. This loss of conductivity modulation in the base is more

severe for cells with a p-type base than for those with an n-type base. This degradation in fill factor at high intensities can be avoided through the use of a low base resistivity. (The highest reported efficiency at high concentration has been obtained in a 0.3 Ω cm base cell.) When the base doping is raised to avoid fill factor degradation, the diffusion length may be reduced to the point where a back-surface field is no longer effective. The degradation of the fill factor can also be reduced by reducing the thickness of the base [19].

3.2. Non-uniform illumination

As the concentration ratio of the system increases, the difficulty of maintaining uniform illumination over the entire area of the cell increases. This leads to an increase in the I^2R losses in the high concentration region. It also causes a portion of the cell to operate in a less than optimum region of the current–voltage (I–V) characteristic [20]. One of the potential advantages of some of the unconventional cell designs to be discussed below is that they are much more tolerant of non-uniform illumination than a conventional design.

4. Conventional cell design

Figure 1 shows a schematic view of a conventional solar cell with one contact made to the grid on the illuminated side of the cell and the other contact made to the back of the cell over the entire area. Most conventional high concentration silicon solar cells include the back-surface diffusion shown in order to provide good ohmic contact and to provide a back-surface field to reduce the loss of minority carriers at the back surface.

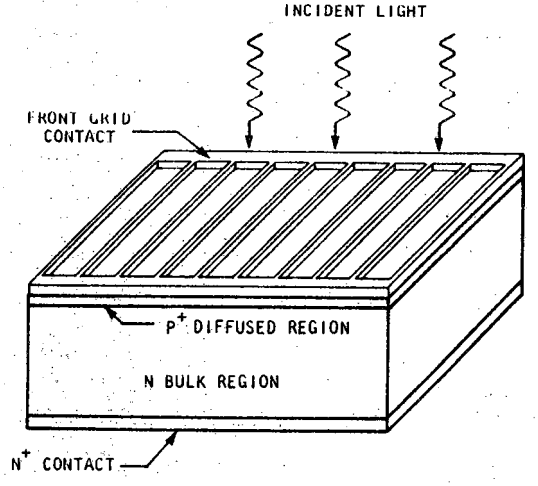

Fig. 1. A conventional high intensity solar cell.

4.1. Emitter design

The parameters which need to be considered in the design of the emitter region are the impurity type, the junction depth, the surface concentration and the surface passivation.

4.1.1. Doping type

In space applications the life of the cell is dominated by the radiation damage which occurs in the base. Since this damage is a minimum for a p-type base, space cells have p-type bases. For terrestrial applications, we are not constrained by radiation damage considerations. The loss of conductivity modulation in the base is less severe in p^+–n cells that in n^+–p cells; this favors a p^+ emitter. However, for a given doping level the sheet resistance will be lower for an n^+ emitter because of the higher mobility of electrons.

In contrast, the minority carrier diffusion length for electrons is longer than for holes. In high concentration cells the base of the cell is frequently operated under high injection conditions, which means that the ambipolar diffusion length, and not the minority carrier diffusion length, applies in the base. Because of the very heavy doping conditions found in the emitter, the emitter is not in high injection and the minority carrier diffusion length applies. This favors the use of a p^+ emitter.

Band gap narrowing effects appear to be comparable for n- and p-type doping, although this is by no means a well-demonstrated fact [21].

In spite of the above comments, for terrestrial applications a clear-cut choice has not emerged for the emitter doping type. Both p^+–n and n^+–p cells have been fabricated with conversion efficiencies of 20% at high concentrations.

The surface concentration of the emitter diffusion is usually kept as high as is compatible with low temperature processing in order to keep the sheet resistance as low as possible. Typical diffusion temperatures are in the vicinity of 850 °C. Typical surface concentrations are $(1 - 3) \times 10^{20}$ cm^{-3}.

Cell processing parameters are chosen to maintain a transparent emitter, *i.e.* an emitter in which minority carriers can move through the entire emitter without recombination. When this condition is attained, the loss of carriers in the emitter is controlled by the surface.

4.2. The base

The design of the base requires a determination of the base thickness, the resistivity and the doping type. The choice of the doping type has already been discussed in the discussion of the emitter design. The choice of the base resistivity is determined by the relationship between the doping level and the lifetime and possible band gap narrowing effects. Fill factor and V_{oc} considerations argue for a low base resistivity, while lifetime considerations argue for a high base resistivity. To date, the highest efficiency cells have been obtained in relatively low resistivity base cells (0.3 Ω cm).

In low base resistivity cells the diffusion length in the base is shorter than in high resistivity cells. In fact, it may be less than 100 μm, the thick-

ness of silicon which is required to generate 90% of the available hole–electron pairs in an air mass one (AM1) spectrum. Under these circumstances, a back-surface field has little effect on cell performance and the thickness of the cell is determined by the ability to process the cell without breakage rather than by the optimum base thickness for electrical purposes. The optimum cell thickness will be in the vicinity of 100 μm with an optically absorbing rear surface and 50 μm with a reflecting rear surface. Typical concentrator cells are at present approximately 300 μm thick.

4.3. The back-surface field

The presence of a high–low junction at the back surface of the cell will create an electrostatic field which will act to keep the minority carriers in the base away from the rear surface. In a cell in which the diffusion length exceeds the base width the presence of this minority carrier mirror will result in an increase in both V_{oc} and I_{sc}. Under low injection conditions, the voltage across the high–low junction is small and the number of minority carriers which reach the high recombination region of the back surface is small. The result is that the short-circuit current is increased because fewer carriers are lost at that surface. This also results in an increase in the open-circuit voltage due to an increase in the number of carriers in the base under open-circuit conditions. Under high injection conditions the minority carrier concentration in the base exceeds the doping level. This causes a voltage to be developed across the high–low junction which adds to the voltage developed at the rectifying junction, increasing V_{oc}. The presence of this voltage across the high–low junction causes minority carriers to be injected into the heavily doped rear region. Thus, at high concentration levels the high–low junction is not as effective as a minority carrier mirror, as at low concentration levels [22].

Because of this loss of containment at high injection levels, the same techniques which are used to reduce the surface recombination at the emitter would be expected to be helpful at the rear surface, *i.e.* reduction of the area covered by metal and passivation of the surface. Some of these techniques, however, are not compatible with the need to make very low thermal and electrical resistance contact with the cell. Some relief from this problem is available if the high–low junction diffusion is made much deeper than the emitter diffusion.

If the diffusion length in the base is small compared with the base width, as is the case for low base resistivity, the back-surface diffusion has little effect other than to afford a means of low resistance contact with the cell. In fact, concentrator cells, which have the highest reported conversion efficiency to date, do not utilize a back-surface field.

5. Unconventional cell designs

Many of the design parameters of a conventional cell are the result of a series of compromises between competing phenomena. The emitter design is

26

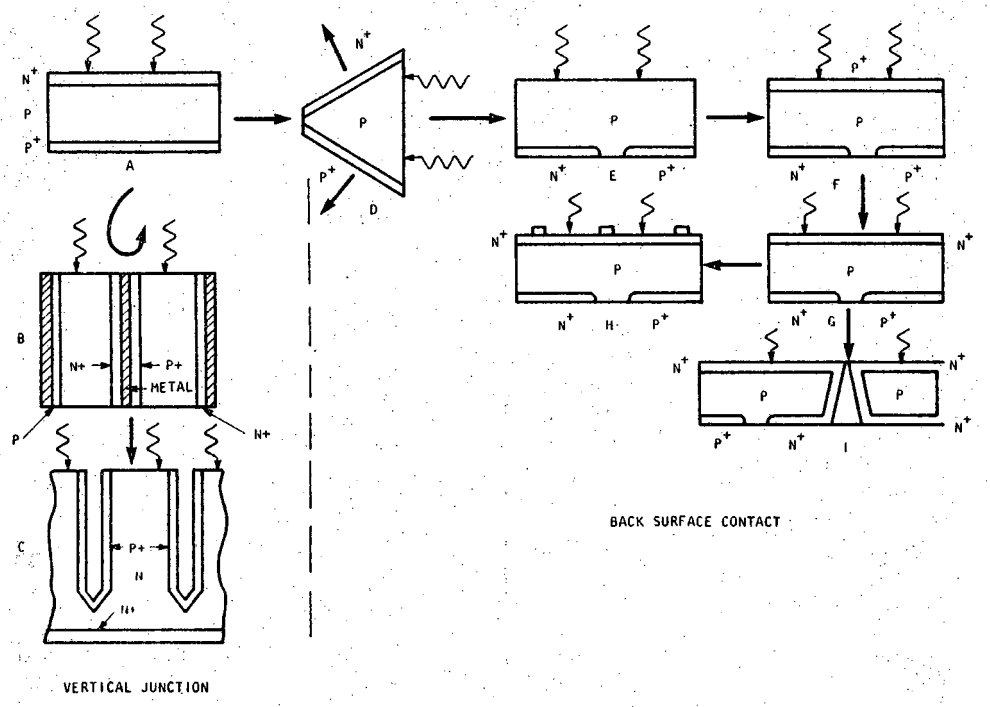

Fig. 2. Unconventional high intensity solar cell designs.

a compromise between the need for a heavily doped deep junction to reduce the sheet resistance of the layer and the need to keep the doping light (to avoid heavy doping effects) and shallow (to increase the collection efficiency of carriers generated near the surface). Similarly, the base design is a compromise: a thick base is desired to absorb long wavelength radiation; a thin base is desired to increase the fill factor. A heavily doped base is needed to maintain a high fill factor at high intensities; a lightly doped base is desired to maintain long diffusion lengths and high collection efficiency. The grid design is a compromise between the need to minimize series resistance and the competing need to minimize shading.

Many cell designs have been proposed which address one or more of these compromises. While the number of designs is large, they may all be viewed as variations of the conventional back-surface field cell as is illustrated in Fig. 2. The cells which are labeled vertical junction may be viewed as resulting from a simple rotation of the cell, such that the illumination path is parallel to the junctions. If additional cells are now placed electrically in series as in Fig. 2(b), the resulting cell is the vertical multijunction (VMJ) cell [23 - 27]. If the vertical junctions are made by means of a directional etch followed by a diffusion, the etched multiple vertical junction cell [2] (Fig. 2(c)) results. If we now return to Fig. 2(a) and visualize the back-surface field cell as being stretched and opened as in Fig. 2(d), we obtain one section of the V-groove cell [28]. If the stretching operation is continued

until the p^+ and n^+ junctions lie in the same plane, the result is one section of the interdigitated back-contact (IBC) cell [29] (Fig. 2(e)). Addition of a high–low diffusion to the illuminated surface results in the front-surface field (FSF) cell [30] (Fig. 2(f)). If a rectifying junction is used instead of a high–low junction, the result is the tandem cell (Fig. 2(g)) [31, 32]. With only the addition of a grid (Fig. 2(h)) this now becomes the double-sided cell [33]. If a hole is etched through the tandem cell, followed by a diffusion which connects the front and rear junctions, the result is the polka dot cell (Fig. 2(i)). Each of these cells has been proposed in order to circumvent one or more of the design compromises which must be made when using the conventional cell design for high intensity applications.

Before we embark on a discussion of the advantages of each of these designs (real or imagined) we should note that none of the designs has received the extensive development effort that has been afforded the conventional cell. Thus the state of the art in these cells is not as well developed as that in the conventional cell. Even so, some of them have already exhibited an excellent high intensity performance and are expected to show significant improvement as further work is performed.

Figure 2 is a useful way in which to view the physical relationship between the various designs, but it does not represent the chronological order in which they were proposed, nor is it particularly useful when we compare the relative merits of the cells. In our discussion of these designs we shall begin with the IBC cell as a convenient starting point.

5.1. Back-surface contact cells

5.1.1. Interdigitated back-contact cell

The IBC cell [29] (Fig. 3) was the first of the back-surface contact cells to be proposed and is still a leading candidate among these types of cell for high intensity applications. It is also the back-surface contact cell for which the most information is available. We shall discuss this cell first and then shall use this cell as a basis for comparison for the other back-surface contact cells.

5.1.1.1. Advantages of the interdigitated back-contact cell. The advantages of the IBC cell design at high intensities over that of a conventional cell are as follows.

(1) No shading of the illuminated surface occurs since there is no grid or contact structure on the illuminated surface. In a conventional high intensity cell the grid structure will shade 5% - 10% of the surface.

(2) The metal contacts, all of which are on the rear surface, may cover nearly the entire surface and may be made as thick as is desired. This means that the series resistance of the contacts may be made as small as is desired and for all practical purposes the metal resistance is eliminated as a problem even at extremely high illumination levels.

(3) The current flows normal to the surface in the diffused regions, rather than parallel to the surface as in a conventional cell (Fig. 4). This

28

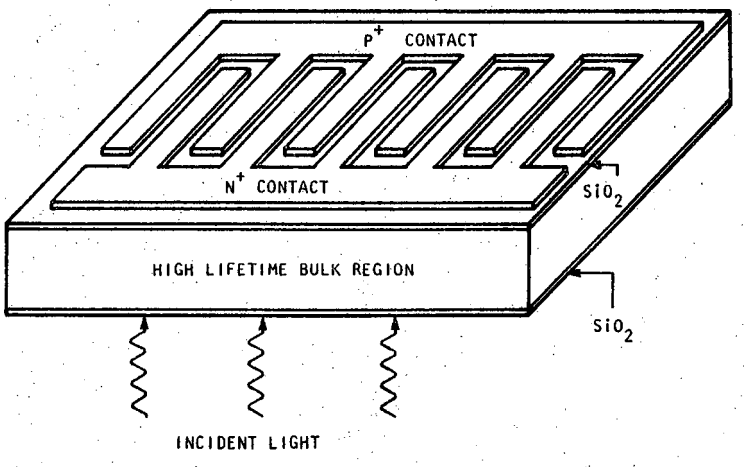

Fig. 3. The IBC cell.

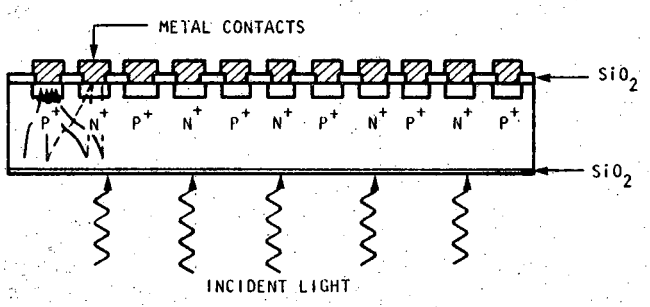

Fig. 4. Sectional view of an IBC cell (— — —, electron flow path; ——, hole flow path).

means that the sheet resistance of the diffused regions is no longer a constraint and the voltage drop in these regions is negligible. The doping density and junction depth do not have to be a compromise in this device.

(4) Because of the reduction of series resistance effects described in (2) and (3), non-uniform illumination degradation effects are much less severe than in a conventional cell.

(5) The junction depth from the diffused surface may be chosen independently of the constraints on short wavelength collection efficiency which dictate a shallow junction in a conventional cell.

(6) The illuminated surface does not contain a diffused layer and as a result the undamaged surface can be fabricated with a low surface state density and correspondingly low surface recombination velocity. The result is that, even though short wavelength radiation creates carriers very near the surface and far from the collecting junctions, the collection efficiency is high and nearly wavelength independent. Figure 5 shows the measured quantum efficiency of an IBC cell [34].

(7) The free carriers are generated, almost entirely, in a region of the cell which is free of diffusion damage and is relatively lightly doped. This is

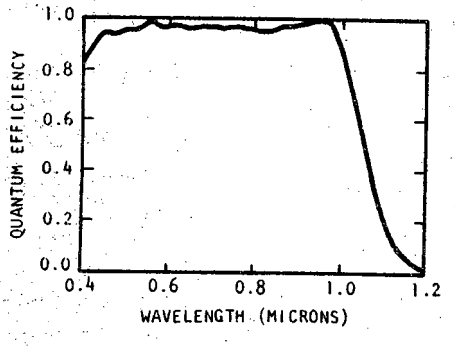

Fig. 5. Quantum efficiency of an IBC cell.

in marked contrast with the situation in the emitter of a conventional cell. This means that the carriers move through a potentially very long lifetime, long diffusion length region without encountering a damaged region prior to reaching the collecting junction. The very long diffusion lengths which are obtained allow the use of a thick cell which results in maximum absorption of the long wavelength portions of the solar spectrum.

5.1.1.2. Problems in the interdigitated back-contact cell design. In order for this cell to operate efficiently, the base diffusion length must be large (of the order of 1000 μm). The result of this is that the cell is sensitive to any damage which may occur at the edge of the cell during the cutting operations which separate the individual cells from the wafer. This problem has been alleviated through the use of laser scribing of the cells.

Also, since the carriers generated by the blue end of the solar spectrum are generated near the surface and far from the collecting junction, the surface recombination must be very low if the cell is to collect these carriers. In an IBC cell these carriers may have to travel 50 - 300 μm before reaching the collecting junctions compared with 0.2 - 0.5 μm for a conventional cell. The reason that this increase of two to three orders of magnitude in the distance which these carriers must travel can be tolerated is that the carriers travel through a region which is undamaged by diffusion or implantation and, under proper processing conditions, will have a very long lifetime and diffusion length compared with that found in the emitter of a conventional device.

In order for silicon cells to operate efficiently at high concentration illumination levels, the cells must be cooled. The IBC cell must be electrically isolated from the heat sink on which it is mounted, and this causes added complications in the design of the mount over that necessary for a conventional cell.

5.1.1.3. Performance of the interdigitated back-contact cell. IBC cells have been operated, in the dark, up to current densities of 20 A cm^{-2} without observation of the presence of series resistance effects. Conversion

efficiencies of 18.1% have been measured at a 30 sun concentration [35]. At the present time the performance of the IBC cell is limited by problems encountered in cooling of the cell. An excellent blue response (Fig. 5) has been observed together with a high quantum yield [34].

5.1.2. The front-surface field and the tandem cells

The FSF cell [30], shown in Fig. 6, is identical with the IBC cell except that the illuminated surface contains a high–low junction. The intent is to provide a built-in field at the surface which will keep minority carriers away from the high recombination surface in the same manner that a back-surface field operates in a conventional cell.

In the tandem cell (Fig. 7) [32] the front-surface high–low junction of the FSF cell is replaced with a rectifying junction. In this case the generation of carriers in this region causes this junction to become forward biased and to inject minority carriers into the base region of the cell. These carriers are then collected at the rear-surface junctions as in the IBC cell. The operation of the tandem cell in this mode is similar to that of an open-base transistor, and in fact the cell has been analyzed in the same manner as a transistor [36]. A contact grid structure can also be placed on the illuminated surface of the tandem cell such that both the front and the rear junctions collect carriers. In this mode the cell operates as a conventional cell with an added collecting junction at the rear for carriers generated deep within the structure. The gain in short-circuit current obtained by this has not been sufficient to overcome the losses due to shading, front-junction and surface recombination, and series resistance to warrant its use at high concentrations.

Tandem cells without a grid structure on the illuminated surface have been operated at insolation levels up to 50 suns. Peak conversion efficiency occurred at 10 suns (AM1) and was found to be 13.2% [32]. To date,

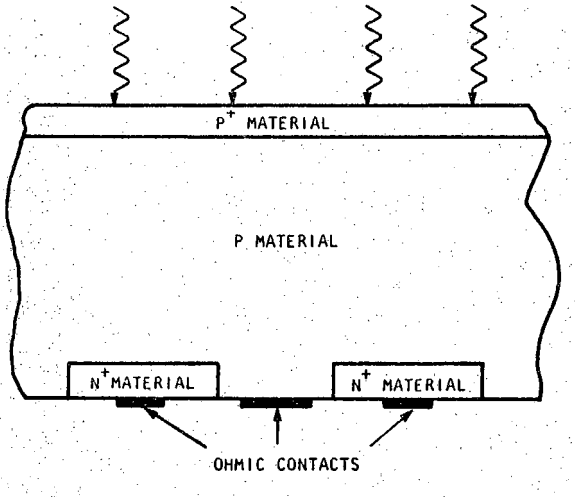

Fig. 6. The FSF cell.

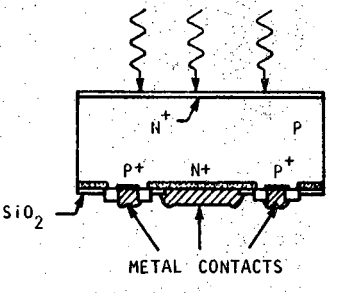

Fig. 7. The tandem cell.

neither the high–low junction nor the p–n junction on the front surface has yielded a blue responsivity which is as good as that of the IBC cell. The effective surface recombination of these types of surfaces has been measured [37]. The high–low junction was found to have an effective surface recombination which was an order of magnitude lower than the p–n junction.

5.1.3. The double-sided cell

The double-sided cell [33] (Fig. 8) is nearly identical with the tandem cell (with a grid on the illuminated surface) in concept and as a result the comments already made about the tandem cell apply to this cell as well. This cell has been proposed for use in a low concentration system in which both sides of the cell are illuminated. The double-sided cell has little promise at high insolation levels.

5.1.4. The polka dot cell

The polka dot cell [38] (Fig. 9) may be viewed as a version of the tandem cell in which the junction on the illuminated surface is contacted by a series of holes which are selectively etched through the cell and which have a diffusion layer which connects the front and rear junctions. This feature allows the junction on the illuminated surface to act as a minority carrier collector without the problems associated with a grid structure. Also, the tapered nature of the contact holes will cause the light striking the edge of the holes to be deflected into the bulk of the cell and not to be lost. This cell should have very little optical loss due to the front-contact structure.

Initial reports on this cell have only dealt with the polka dot cell's performance at 1 sun. The 1 sun efficiency was only 10.5% because of a

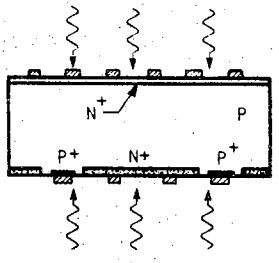

Fig. 8. The double-sided cell.

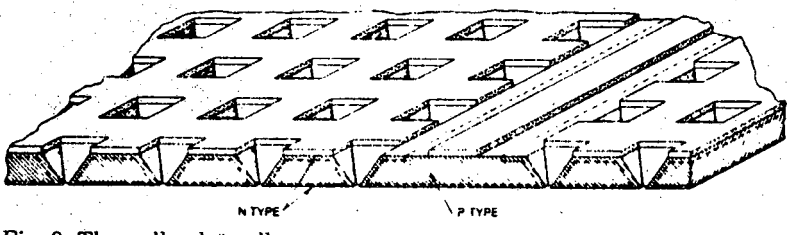

Fig. 9. The polka dot cell.

32

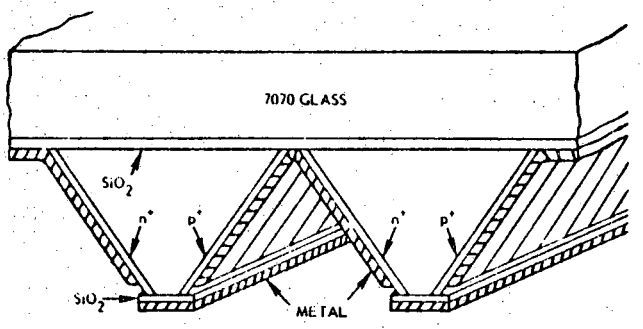

Fig. 10. The V-groove cell.

low minority carrier lifetime and a high series resistance. With proper design and sufficient metallization it should exhibit a performance which is slightly better than that of the tandem cell as it incorporates all the desirable features of that cell as well as front-surface collection and internal optical reflection.

5.1.5. The V-groove cell

The V-groove cell [28] (Fig. 10) is also obtained by using a selective etch to make, in this case, triangular cross-sectional grooves in the unilluminated side of the cell which contain a p^+ region on one wall of the groove and an n^+ region on the other wall. One advantage of the V-groove cell is that the path length over which the carriers have to travel to be collected is, on the average, shorter than for the IBC cell of comparable dimensions. Also, if the walls of the groove are reflecting, light striking the groove walls will be deflected into the bulk of the cell.

The theoretical performance of the cell has been discussed by Chappell [28]. He has predicted that the cell will be capable of a conversion efficiency of over 20% at 300 suns (27 °C). The measured value under these conditions was 12.2%.

Other potential advantages of this structure are the environmental protection offered by the 7070 glass front surface and the simple one-mask fabrication procedure which is possible.

5.2. Vertical junction cells

5.2.1. The vertical multijunction cell

The VMJ cell [23] (Fig. 11) may be thought of as a series-connected set of back-surface field cells which are illuminated from the side. One primary advantage of this cell is that the current generated per cell is small and, since the cells are connected in series, the cell is a low current, high voltage device. As such, it does not suffer from series resistance problems at high concentration levels as would a conventional cell. The metal interconnecting layers still represent an optical loss which is proportional to their thickness. This thickness may be quite small, however.

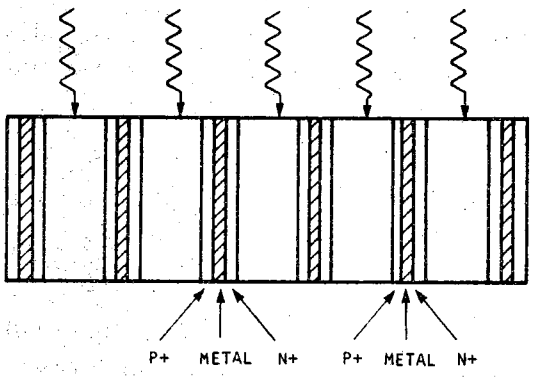

Fig. 11. The VMJ cell.

One disadvantage of the series-connected version of the VMJ cell is that it is quite sensitive to illumination non-uniformities across the cell in a direction perpendicular to the junctions. It is possible to use various series and parallel interconnection schemes to help to alleviate this problem at the expense of an increase in complexity. Surface passivation is also more difficult in this cell as this must be accomplished after metallization and therefore must be a low temperature process.

The optical generation of free carriers will be a non-uniform function of distance from the surface. The junctions will try to remain as equipotentials. This will cause carriers to be extracted from the top of the cell and injected into lower portions of the cell, resulting in a small circulating current within the device. The effect is not large and should only result in a loss of the order of kT/q in the open-circuit voltage.

These cells have been operated at high intensities (2 - 20 W cm^{-2}) with the result that the peak efficiency occurred at 10 W cm^{-2}. It was also observed that the temperature dependence of V_{oc} decreased substantially at high concentration levels.

5.2.2. The etched vertical junction cell

The etched vertical junction cell [2] (Fig. 12) utilizes a selective etch to form nearly vertical walled narrow grooves which are then diffused to form the vertical junctions. The high–low junction is formed on the back surface.

Cells of this type which have been fabricated to date have had the grooves connected in parallel, although it is possible to have a series-connected configuration. Figure 13 shows a further modification of this design in which a second set of grooves is etched from the other side to form the double-etched vertical junction cell. This cell should have a higher fill factor than the etched vertical junction cell.

These cells are similar to the VMJ cell in that the grooves may be spaced very close together so that high collection efficiencies are possible without extremely long diffusion lengths. Since the illuminated surface does not contain a diffused layer, it can be passivated very well and, since passiva-

34

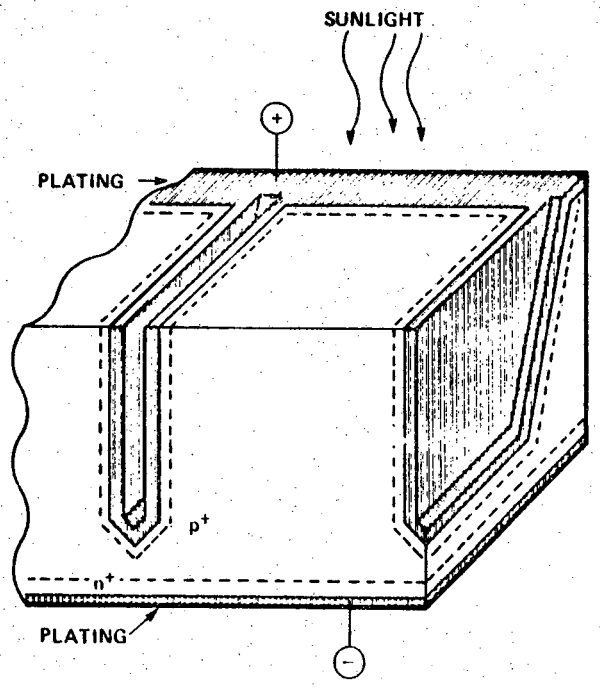

Fig. 12. The etched vertical junction cell.

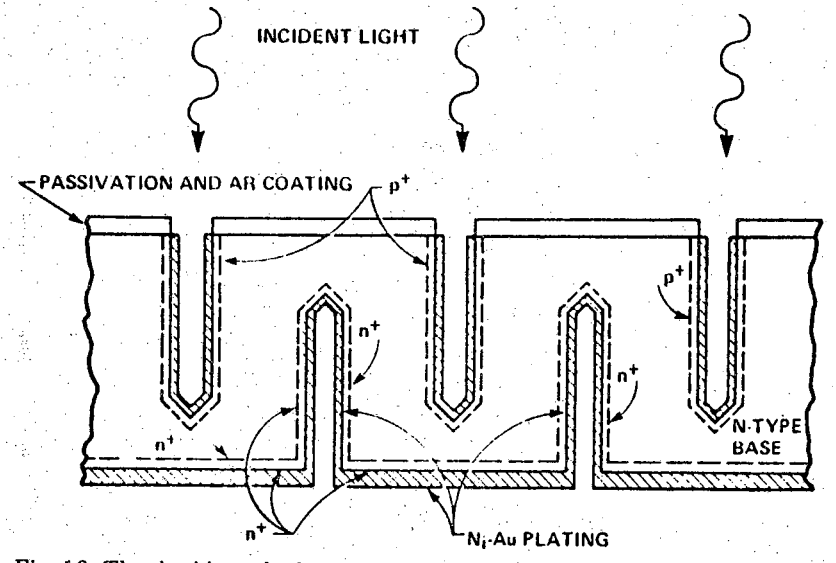

Fig. 13. The double-etched vertical junction cell (AR, antireflection).

tion can occur before metallization, the passivation difficulties encountered in the VMJ cell are avoided.

The measured performance of this cell has been excellent at extremely high intensities. Operating efficiencies of 18.5% at 600 suns have been reported. Cells of this type have been operated up to concentration ratios of

TABLE 1

Property	*Cell design*								
	Conventional	*IBC*	*Tandem*	*FSF*	*Double-sided*	*V-groove*	*VMJ*	*Etched VMJ*	*Polka dot*
No shading		X	X	X		X[a]	X[a]	X[a]	X[a]
Thick large-area metal		X	X	X		X	X[b]	X	X
Current flow normal to diffused surface		X	X	X		X	X	X	
Good tolerance for non-uniform illumination		X	X	X		X[c]		X[c]	X
Junction depth and doping not compromised by sheet resistance		X	X	X		X	X	X	
Low surface recombination velocity on illuminated surface		X	X[d]	X[d]		X		X	X[d]
Optical path longer than diffusion path					X	X	X	X	X

[a]Some loss of active area occurs as a result of the structure. The effect should be smaller than that for a conventional grid structure.
[b]If the device is series connected, the metal thickness should be minimized.
[c]This is true only for a parallel-connected configuration. A series-connected configuration will not be tolerant.
[d]The front surface will have a high surface recombination velocity but this will be somewhat alleviated by the presence of built-in fields.

1000. The cells have been shown to be very tolerant of non-uniform illumination. They have also exhibited a decrease in the value of $(1/V_{oc})(dV_{oc}/dT)$ by a factor of 2 as the intensity varied from 1 to 1000 suns [2].

5.2.3. A comparison of the unconventional cell designs

Table 1 compares the features of the various concentrator cell designs. As can be seen by examination of this table, each of these designs has potential advantages over a conventional cell design at high concentrations. All the high concentration cell designs have managed to circumvent, in one way or another, the problem of series resistance. All designs require long diffusion lengths for high efficiency operation, although the demands in this respect are less for those cells with the optical path longer than the diffusion path. Some of the designs have eliminated the shading problem altogether. In some of the designs, illuminated surface recombination has been reduced from that found in a conventional cell by avoiding the presence of diffusion on the illuminated surface.

36

6. The future of silicon high concentration cells

The amount of development effort which has been expended on the various cell designs discussed here has not been uniformly distributed, and therefore the conversion efficiency values quoted, some of which are quite old, should not be taken as representing the ultimate performance of that design. Even though the amount of work which has gone into these unconventional designs is much less than for the conventional cell, their performance is comparable with the conventional cell for midrange concentration and already exceeds it for the high concentration range.

One of the problems with the use of silicon in a high concentration system is the fact that it has (at low insolation levels) a rapid fall in operating efficiency as the temperature increases. However, the observed decrease in this effect at high insolation levels may alleviate this problem somewhat.

The demonstrated ability of silicon cells to operate at very high concentrations also makes them a prime candidate as one of the cells in split spectrum multiple-band-gap systems.

References

1 H. T. Weaver, R. D. Nasby and C. M. Garner, Effects of design and process variations on silicon concentrator solar cell performance, *Proc. Int. Electron Devices Meet., Washington, DC, December 8 - 10, 1980*, IEEE, New York, 1980, p. 190.

2 R. I. Frank, J. L. Goodrich and R. Kaplow, A low series resistance silicon photovoltaic cell for high intensity applications, *Proc. 14th Photovoltaic Specialists' Conf., San Diego, CA, January 7 - 10, 1980*, IEEE, New York, 1980, p. 423.

3 A. Herchakowski, Solar photovoltaic systems using concentrators, *Proc. 19th Power Sources Conf., Fort Monmouth, NJ, May 18 - 20, 1965*, pp. 170 - 173.

4 W. A. Beckman, P. Schoffer, W. R. Hartman, Jr., and G.O.G. Lof, Design considerations for a 50-watt photovoltaic power system using concentrated solar energy, *Sol. Energy, 10* (3) (1966) 132 - 136.

5 E. L. Ralph, Use of concentrated sunlight with solar cells for terrestrial applications, *Sol. Energy, 10* (2) (1966) 67 - 71.

6 H. Tabor, Mirror boosters for solar collectors, *Sol. Energy, 10* (3) (1966) 111 - 118.

7 M. S. Lundstrom, R. J. Schwartz and J. L. Gray, Transport equations for the analysis of heavily doped semiconductor devices, *Solid-State Electron., 24* (1980) 195.

8 P. A. Iles, Increased output from silicon solar cells, *Proc. 8th Photovoltaic Specialists' Conf., Seattle, WA, August 1970*, IEEE, New York, 1970, p. 345.

9 H. W. Brandhorst, Jr., Silicon solar cell efficiency — practice and promise, *Proc. 9th Photovoltaic Specialists' Conf., Silver Springs, MD, May 2 - 4, 1972*, IEEE, New York, 1972.

10 A. H. Marshak, M. A. Shibib, J. G. Fossum and F. A. Lindholm, Rigid band analysis of heavily doped semiconductor devices, *IEEE Trans. Electron Devices, 28* (3) (1981) 293 - 298.

11 M. P. Godlewski, H. W. Brandhorst, Jr., F. A. Lindholm and C. T. Sah, Experimental investigation of the excess charge and time constant of minority carriers in the thin diffused layer of 0.1 ohm-cm silicon solar cells, *Materials Research Conf., June 23 - 25, 1976.*

12 H. P. D. Lanyon and R. A. Tuft, Bandgap narrowing in heavily doped silicon, *Tech. Dig. Int. Electron Devices Meet., Washington, DC, December 4 - 6, 1978*, IEEE, New York, 1978, pp. 316 - 319.

13 J. G. Fossum, F. A. Lindholm and M. A. Shibib, The importance of surface recombination and energy bandgap narrowing in p–n junction silicon solar cells, *IEEE Trans. Electron Devices, 26* (9) (1979) 1294 - 1298.
14 C. R. Baraona and H. W. Brandhorst, Jr., *Proc. 11th Photovoltaic Specialists' Conf., Phoenix, AZ, May 6 - 8, 1975*, IEEE, New York, 1975, p. 44.
15 P. A. Iles and S. I. Socolof, Effect of impurity doping concentration on solar cell output, *Proc. 11th Photovoltaics Specialists' Conf., Phoenix, AZ, May 6 - 8, 1975*, IEEE, New York, 1975, p. 19.
16 R. J. Handy, Theoretical analysis of the series resistance of a solar cell, *Solid-State Electron., 10* (1967) 765.
17 C. M. Garner, Extrinsic losses in solar cells for linear focus systems, *SAND Rep. 79-1781 (D)*, 1979 (Sandia National Laboratories, Albuquerque, NM).
18 W. T. Matzen, S. Y. Chiang and B. Carbajal, Optimized metallization patterns for large-area silicon solar cells, *Proc. 12th Photovoltaic Specialists' Conf., Baton Rouge, LA, November 15 - 18, 1976*, IEEE, New York, 1976, p. 340.
19 R. J. Schwartz, M. S. Lundstrom and R. D. Nasby, The degradation of high-intensity BSF solar-cell fill factors due to a loss of base conductivity modulation, *IEEE Trans. Electron Devices, 28* (1981) 264.
20 R. D. Nasby and C. M. Garner, Effects of nonuniform illumination on the performance of silicon concentrator solar cells, *Proc. 14th Photovoltaic Specialists' Conf., San Diego, CA, January 7 - 10, 1980*, IEEE, New York, 1980, p. 437.
21 A. W. Wieder, Emitter effects in shallow bipolar devices: measurements and consequences, *IEEE Trans. Electron Devices, 27* (1980) 1402 - 1408.
22 J. G. Fossum, R. D. Nasby and S. C. Pao, Physics underlying the performance of back-surface-field solar cells, *IEEE Trans. Electron Devices, 27* (4) (1980) 785 - 791.
23 B. L. Sater, *Proc. 11th Photovoltaic Specialists' Conf., Phoenix, AZ, May 6 - 8, 1975*, IEEE, New York, 1975.
24 C. Goradia and B. L. Sater, A first order theory of the p^+–n–n^+ edge-illuminated silicon solar cell at very high injection levels, *IEEE Trans. Electron Devices, 24* (4) (1977) 342 - 351.
25 B. L. Sater, H. W. Brandhorst, Jr., T. J. Riley and R. E. Hart, Jr., The multiple junction edge illuminated solar cell, *Proc. 10th Photovoltaic Specialists' Conf., Palo Alto, CA, November 13 - 15, 1973*, IEEE, New York, 1974, p. 188.
26 C. Goradia, R. Ziegman and B. L. Sater, Characteristics of high intensity (HI) edge-illuminated multijunction silicon solar cells — experimental results and theory, *Proc. 12th Photovoltaic Specialists' Conf., Baton Rouge, LA, November 15 - 18, 1976*, IEEE, New York, 1976, p. 781.
27 R. I. Frank and R. Kaplow, Improved performance of solar cells for high intensity applications, *Proc. 12th Photovoltaic Specialists' Conf., Baton Rouge, LA, November 15 - 18, 1976*, IEEE, New York, 1976, p. 820.
28 T. I. Chappell, The V-groove multijunction solar cell, *Proc. 13th Photovoltaic Specialists' Conf., Washington, DC, June 5 - 8, 1978*, IEEE, New York, 1978, p. 791.
29 M. D. Lammert and R. J. Schwartz, The interdigitated back contact solar cell: a silicon solar cell for use in concentrated sunlight, *IEEE Trans. Electron Devices, 24* (4) (1977) 337 - 342.
30 O. Von Roos and B. Anspaugh, The front surface field solar cell, a new concept, *Proc. 13th Photovoltaic Specialists' Conf., Washington, DC, June 5 - 8, 1978*, IEEE, New York, 1978, p. 1119.
31 S. Y. Chiang, B. G. Carbajal and G. F. Wakefield, Thin tandem junction solar cell, *Proc. 13th Photovoltaic Specialists' Conf., Washington, DC, June 5 - 8, 1978*, IEEE, New York, 1978, p. 1290.
32 S. Y. Chiang, B. G. Carbajal and G. F. Wakefield, Concentrator solar cell assembly, *Proc. 1978 Annu. Meet. of the International Solar Energy Society, American Section, Denver, CO, August 1978*, International Solar Energy Society, American Section, Newark, DE, 1978, p. 342.

38

33 A. Cuevas, A. Luque and J. M. Ruiz, A n^+–p–n^+ double-sided solar cell for optimal static concentration, *Proc. 14th Photovoltaic Specialists' Conf., San Diego, CA, January 7 - 10, 1980*, IEEE, New York, 1980, p. 76.
34 C. M. Garner, R. D. Nasby and F. W. Sexton, An interdigitated back contact solar cell with high-current collection, *Proc. 15th Photovoltaic Specialists' Conf., Orlando, FL, May 1981*, IEEE, New York, 1981.
35 C. M. Garner, personal communication, May 1981.
36 W. T. Matzen, S. Y. Chiang and B. G. Carbajal, A device model for the tandem junction solar cell, *IEEE Trans. Electron Devices, 26* (1979) 1365.
37 T. Daud and T. J. Cheng, Surface recombination velocity measurement for silicon solar cells, *Proc. 15th Photovoltaic Specialists' Conf., Orlando, FL, May 1981*, IEEE, New York, 1981.
38 R. N. Hall and T. J. Soltys, Polka-dot solar cell, *Proc. 14th Photovoltaic Specialists' Conf., San Diego, CA, January 7 - 10, 1980*, IEEE, New York, 1980, p. 550.

APPENDIX B

This appendix contains a paper presented at the Space Photovoltaics Research and Technology Conference at NASA-Lewis in October 1983 [5].

TWO-DIMENSIONAL COMPUTER SIMULATION OF EMVJ AND GRATING SOLAR CELLS UNDER AMO ILLUMINATION

J. L. Gray and R. J. Schwartz
School of Electrical Engineering
Purdue University
West Lafayette, Indiana

The design of photovoltaic cells for space applications can be a difficult task since these devices must be designed for "end-of-life" operation. The degradation of minority carrier diffusion length due to radiation damage can make the end-of-life performance of a cell radically different from its as fabricated performance. In order to experimentally evaluate the end-of-life performance of a cell, it must be irradiated in the laboratory to simulate the effects of a space environment. However, this procedure of design, fabrication, evaluation, and redesign can be very time consuming. In addition, it is often difficult to determine which design parameter is responsible for a change in cell performance. Even variations in wafer characteristics and processing parameters can be difficult to trace and therefore introduce uncertainties in cell evaluation. Because so many uncertainties are involved, the determination of an optimum cell design is no easy matter.

Most of these difficulties can be eliminated by making use of detailed solar cell simulation programs. A particular design change can be studied with the absolute certainty that nothing else has changed. The effects of radiation damage can be studied merely by altering the carrier diffusion length and redoing the computer simulation. In addition, since the simulation will solve for the electrostatic potential and hole and electron concentrations throughout the interior of the device, one can peer inside the cell itself and "see" where recombination occurs, how the current flows, whether the back-surface-field is effective, etc. Since most cell structures are two-dimensional in nature, a code which solves the semiconductor equations in two-dimensions is necessary in order to best simulate the various devices. All this can be accomplished much more quickly than a device can be fabricated. Therefore, as an aid to designing cells, such a computer code can be invaluable.

In this paper, a computer program, SCAP2D (Solar Cell Analysis Program in 2-Dimensions), is used to evaluate the Etched Multiple Vertical Junction (EMVJ) and grating solar cells. It should be noted that it is only our aim to demonstrate how SCAP2D can be used to evaluate cell designs and that the cell designs studied are by no means optimal designs.

THE SCAP2D PROGRAM

The SCAP2D program solves the three coupled, nonlinear partial differential equations, Poisson's Equation and the hole and electron continuity equations, simultaneously in two-dimensions using finite differences to discretize the equations and Newton's Method to linearize them. The variables solved for are the electrostatic potential and the hole and electron concentrations. Each linear system of equations is solved directly by Gaussian Elimination. Convergence of the Newton Iteration is assumed when the largest correction to the electro-

static potential or hole or electron quasi-potential is less than some predetermined error, typically 10^{-6} kT. A typical problem involves 2000 nodes with a Jacobi matrix of order 6000 and a bandwidth of 243.

The metal-semiconductor contacts are assumed to be ideally ohmic; that is, charge neutrality prevails and both carriers retain their equilibrium values. Other interfaces are described by a Hall-Shockley-Read formulation of surface recombination and by a fixed surface charge density.

Bandgap narrowing is taken into account as described in Ref. 1 and a Caughey-Thomas formulation of carrier mobility is used. Auger and a single trap HSR bulk recombination mechanism are assumed.

SCAP2D SIMULATION RESULTS

The SCAP2D program has been used to examine the effects of radiation damage, simulated by reducing the carrier diffusion lengths, on the operation of the EMVJ and grating solar cells. Simple schematics of these devices are shown in Figures 1 and 2. It can be seen that the grating cell is just a special case of the EMVJ cell in which the depth of the etched groove is zero. In order to keep the comparisons simple, the only design parameters which were varied were cell thickness, etched groove depth, and grid spacing. In addition, so that the shadowing factor is constant, it is assumed that the etched groove width is such that shadowing is 5% for each device.

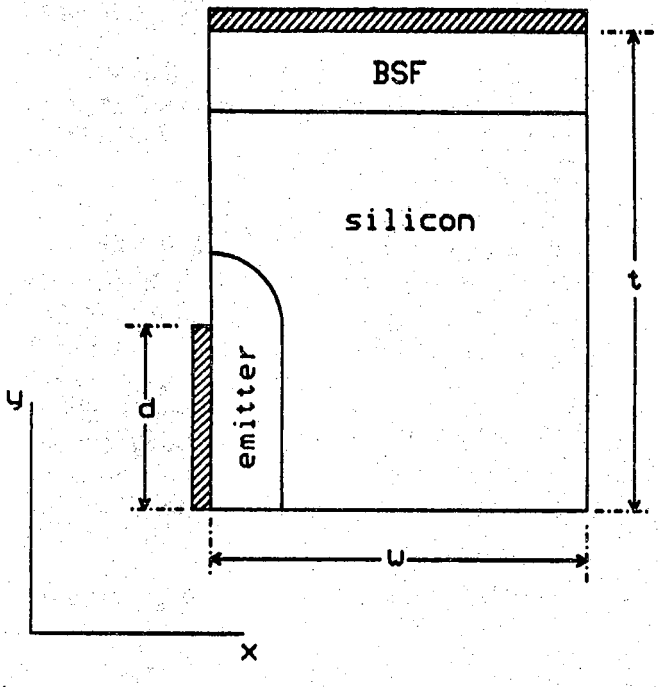

Figure 1. - Schematic of the EMVJ cell used for the SCAP2D simulations.

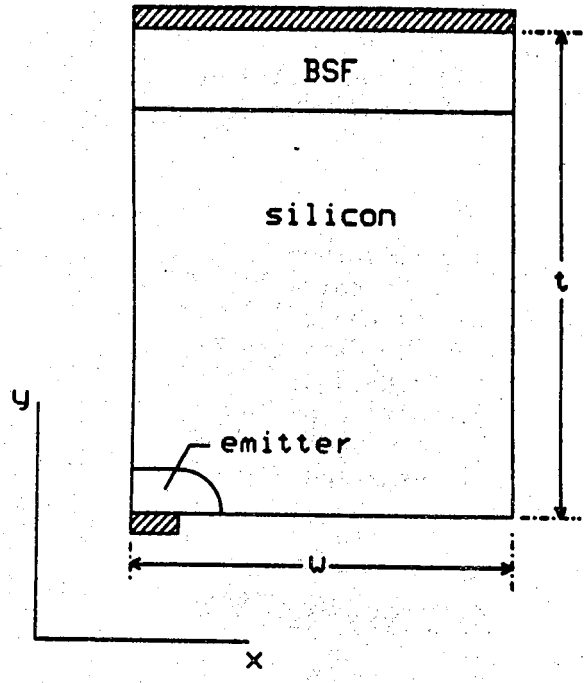

Figure 2. - Schematic of the grating cell used for th SCAP2D simulations.

TABLE 1. - DEVICE PARAMETERS

	Device	t	w	d
1	EMVJ	250μm	125μm	100μm
2	EMVJ	250μm	25μm	100μm
3	EMVJ	75μm	25μm	25μm
4	Grating	75μm	25μm	0
5	Grating	250μm	25μm	0

The remaining design parameters are held fixed as follows. All doping profiles are complimentary error functions with junction depths of 3 microns. The emitter profile has a surface concentration of 1.5×10^{20} cm^{-3} while the back-surface-field (BSF) has a surface concentration of 3×10^{20} cm^{-3}. The base has a resistivity of about 10 ohm-cm. A fixed charge density of 10^{12} charges per cm^2 is assumed at the illuminated surface which has a flatband surface recombination velocity of 1000 cm/sec. Minority carrier diffusion lengths of from 35 to 800 microns were used in the simulations. The simulations were performed for an AM0 solar spectrum with an incident power of 135 mW/cm^2. A perfect anti-reflective coating is assumed.

In Table 1 the simulated devices are described in terms of the three variable parameters: t, the device thickness, w, the grid half spacing, and d, the etched groove depth. Tabulated results of the simulations, giving the open-circuit voltage, short-circuit current, fill factor, efficiency, and collection efficiency, are listed in Table 2 for different values of minority carrier diffusion length.

One fact that is immediately evident is that for long diffusion lengths, the EMVJ cell shows no advantage over the grating cell. Indeed, for a minority carrier diffusion length of 350 microns, cell design has almost no effect on cell efficiency. This is to be expected since all the critical device dimensions are less than a diffusion length. For example, comparing Devices 3 and 4, which have comparable overall dimensions, for a minority carrier diffusion length of 350 microns, we see that there is no advantage to having etched groove junctions. In fact, since the emitter volume is so much larger in the EMVJ cell as compared to the grating cell, there is more recombination and the open-circuit voltage is reduced. As the diffusion length is reduced, however, the advantages of an etched junction become apparent. The purpose of the etched groove is to provide a collecting junction close to any generated excess carrier. For carriers to be efficiently collected, they should be generated within about a diffusion length of the junction or they may recombine before they can be collected. The EMVJ cell allows carriers generated deep within the device to be collected. In the grating cell these carriers have a greater distance to diffuse in order to be collected, and therefore more of them recombine and are lost. For a minority carrier diffusion length of 35 microns, the EMVJ cell (Device 3) is superior to the grating cell (Device 4). This is due to the greater collection efficiency of the EMVJ cell. Thus, for high end-of-life efficiency, a deep etched groove junction is desirable.

TABLE 2. - SCAP2D SIMULATION RESULTS

[L is minority carrier diffusion length.]

		V_{OC}(volts)	J_{SC}(mA/cm^2)	η (%)	FF	η_{coll} (%)
L = 800μm	1	.628	46.3	17.4	.808	98.4
	2	.598	45.8	16.3	.807	97.2
	3	.624	42.9	16.3	.823	97.3
L = 350μm	1	.608	44.7	15.7	.778	94.9
	2	.587	45.6	15.6	.785	97.0
	3	.619	42.8	15.8	.804	97.1
	4	.635	44.4	16.1	.789	98.3
	5	.616	45.4	15.8	.764	96.4
L = 110μm	1	.530	33.7	10.4	.783	71.6
	2	.528	44.7	13.6	.779	95.1
	3	.571	42.2	13.8	.773	95.6
	4	.571	40.7	13.2	.771	92.3
	5	.539	39.9	12.3	.773	84.7
L = 35μm	1	.471	14.7	4.0	.772	33.2
	2	.469	40.6	10.8	.767	86.3
	3	.471	37.4	10.6	.782	84.8
	4	.498	29.7	8.4	.766	67.3
	5	.495	29.6	8.2	.756	62.9

Another critical parameter for end-of-life performance is the grid spacing. As long as the spacing is shorter than a diffusion length, cell performance is not very dependent on this parameter. This can be seen by comparing Devices 1 and 2 for diffusion lengths of 350 and 800 microns. The improved performance of Device 1, though it has a larger grid spacing than Device 2, is again due to the different relative emitter volumes. For short diffusion lengths, however, the difference in performance is dramatic. For Device 1, with a grid half spacing of 125 microns, most of carriers generated between the grid lines are too far from the junction to be collected efficiently. Therefore, it is important to keep the grid half spacing less than the expected end-of-life diffusion length.

Cell performance is least sensitive to the device thickness. When a device has a back-surface-field, two competing effects determine the optimum thickness. The device needs to be thick enough so that nearly all the incident photons with sufficient energy generate electron-hole pairs, and the device needs to be thin enough so that the BSF barrier will be effective. In order for the BSF to be effective, the thickness of the device must be less than a diffusion length. If the end-of-life diffusion length is expected to be much less than 100 microns, devices thin enough to make the BSF work may not be practical.

In Figure 3, the minority carrier concentration in the base of Device 3 is shown for a diffusion length of 800 microns. The illuminated surface is along the x-axis at $y = 0$. The collecting contact is parallel to the y-axis. We can see that the BSF is very effective at containing the minority carriers in this case as the carrier concentration is nearly constant throughout the base region. Looking at the same device for a diffusion length of 35 microns in Figure 4, the back-surface-field is not effective since the minority carriers tend to recombine before they encounter the BSF. Both figures show the minority carrier concentration at the maximum power point.

CONCLUSIONS

Using a detailed simulation program, SCAP2D, the effects of radiation damage, as simulated by changing the minority carrier diffusion length, on EMVJ cell design were studied. The design parameters examined were device thickness, grid half spacing, and etched groove junction depth. For long diffusion lengths, cell performance was relatively insensitive to these parameters. End-of-life (small minority carrier diffusion length), was found to be very sensitive to both the grid half spacing and to the etched groove depth. These parameters must be chosen so that most carriers are generated within a diffusion length of the collecting junction. Because end-of-life diffusion lengths are small, BSF's do not greatly improve cell performance, and therefore end-of-life design is not very sensitive to cell thickness.

REFERENCE

1. M. S. Lundstrom; R. J. Schwartz; and J. L. Gray: Transport Equations for the Analysis of Heavily Doped Semiconductor Devices. Solid-State Electronics, Vol. 24, 1981, pp. 195-202.

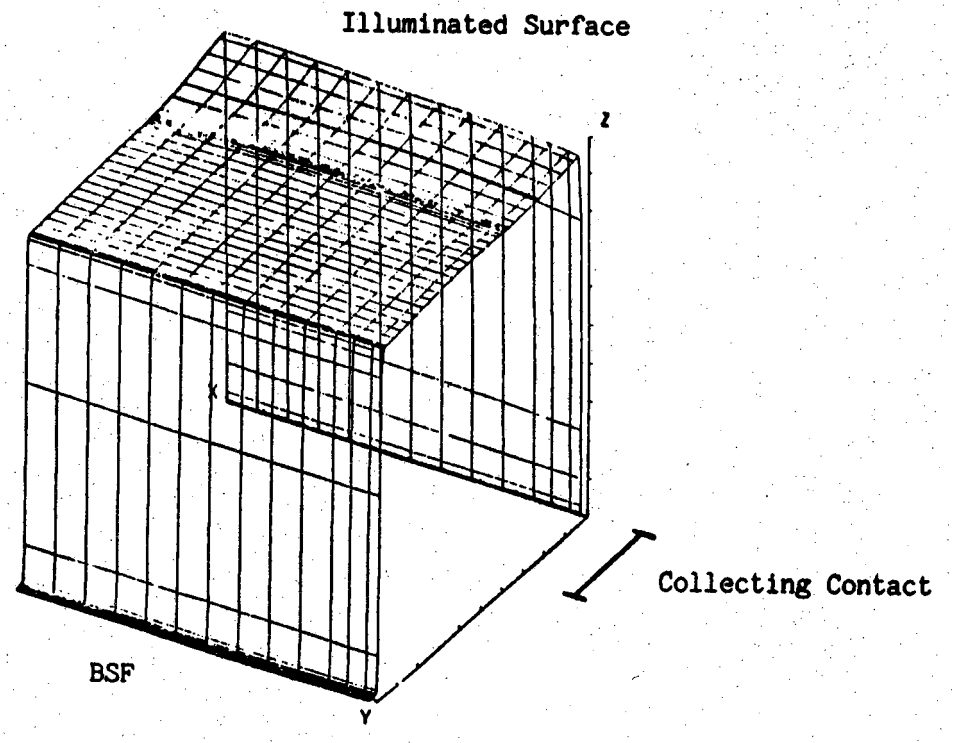

x-axis: 5 to 25 microns
y-axis: 0 to 75 microns
z-axis: 0 to 3×10^{15} cm^{-3}

Figure 3. - Minority carrier concentration within the base of Device 3 operating at the maximum power point with a minority carrier diffusion length of 800 μm. The x and y axes have the same meaning as in Fig. 1. The z-axis is the minority carrier concentration.

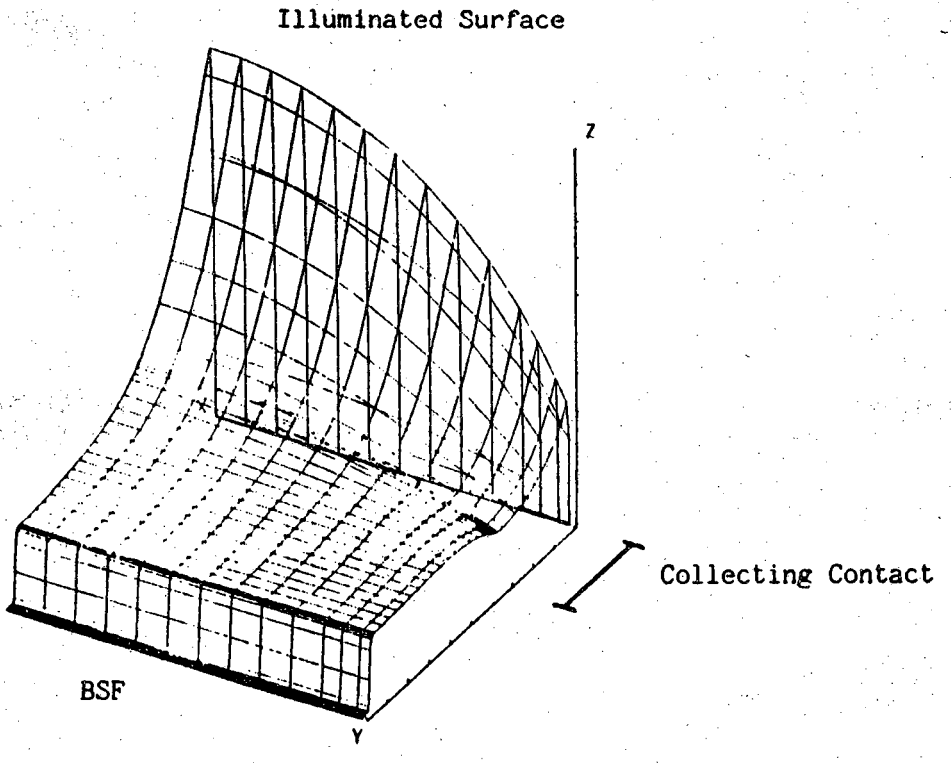

x-axis: 5 to 25 microns
y-axis: 0 to 75 microns
z-axis: 0 to $3 \times 10^{14} cm^{-3}$

Figure 4. - Minority carrier concentration within the base of Device 3 operating at the maximum power point with a minority carrier diffusion length of 35 μm.

APPENDIX C

This appendix contains a paper which appeared in *Solar Cells* [6].

Solar Cells, *12* (1984) 197 - 203

PERFORMANCE LIMITS OF SILICON CONCENTRATOR CELLS

R. J. SCHWARTZ and J. L. GRAY

School of Electrical Engineering, Purdue University, West Lafayette, IN 47907 (U.S.A.)

Summary

In this paper the phenomena which limit the performance of concentrator cells are examined. These include contact grid shadowing, reflective losses, series resistance and recombination mechanisms. These phenomena are examined individually to determine whether and how their effects on cell performance can be reduced or eliminated. It is concluded that, contrary to popular belief, a significant improvement in cell efficiency may yet be realized. Efficiencies approaching 30% under air mass 1.5 illumination at 300 suns appear to be feasible with properly designed cells. One such possible cell design is proposed.

1. Introduction

From a technical point of view, one of the attractive features of working on concentrator solar cells, particularly for very high concentrations, is the fact that cell cost has the potential of being a small fraction of the total system cost and therefore allows the design and fabrication of these cells in a way that would be prohibitively expensive if attempted in a flat-plate cell. This is particularly true for procedures which can increase the efficiency of the cells, since the cost of power generation is inversely proportional to cell efficiency, and relatively modest gains in cell efficiency result in major systems' cost savings.

In the spirit of this special issue which features speculations and forecasts in photovoltaics, we shall examine the problem of silicon high concentration solar cells from two perspectives. The first of these involves examining the present state of the art of silicon high concentration solar cells for insight into those features and phenomena which are at present limiting the performance of these cells. The second approach will be to speculate on which of these limiting factors might be expected to be overcome and which of them are fundamental and are therefore unlikely to be overcome so that we can project possible future performance limits for silicon concentrator cells. We close by speculating on the future design of these cells.

0379-6787/84/$3.00

198

2. Today's best cells

It is interesting to observe that the silicon cells with the highest conversion efficiency at 1 sun are those which were designed for high efficiency at high concentrations and only coincidentally was it observed that these cells also yielded very high 1 sun conversion efficiencies (18% at air mass 1). As a starting point for our speculation, it is instructive to examine the design and performance of present high efficiency cells for guidance as to where further improvements might be obtained and how design features might be changed to achieve these improvements.

Table 1 is a tabulation of the factors which are at present limiting the performance of today's conventional silicon concentrator cells. These are cells which have exhibited conversion efficiencies in excess of 20% at

TABLE 1

Factors which limit the performance of today's high efficiency high concentration conventional solar cells

Limiting effect	*Effect on cell performance*	*Comments*
Shadowing	J_{sc} reduced by about 5%	May be reduced to zero with back-contact cells
Reflection	J_{sc} reduced by 8% - 10%	Coated textured surface could reduce this to 2% - 5%
Series resistance Grid Emitter Base	Fill factor reduced from possible value of 0.84 - 0.87 to observed value of 0.83 or less, depending on intensity	Resistive effects can be made insignificant with non-conventional cell designs
Contact recombination	V_{oc} reduced by 60 - 80 mV from value expected if base recombination dominates and best attainable lifetime *versus* doping values used	May be reduced by reducing contact area and through the use of high–low junctions or heterojunctions
Surface recombination	V_{oc} reduced by 60 - 80 mV from value expected if base recombination dominates and best attainable lifetime *versus* doping values used	Non-conventional cell designs require better surface passivation than conventional cells. Possible use of hydrogen implant warranted for very high efficiency cells
Bulk recombination	V_{oc} reduced by 60 - 80 mV from value expected if base recombination dominates and best attainable lifetime *versus* doping values used	The lifetime in lightly doped Si appears to be limited to 500 - 1000 μs. For heavily doped Si and at very high carrier concentrations, Auger recombination limits performance. Limits appear to be fundamental

concentrations in the range 50 - 100 suns. Both n on p and p on n cells have been shown to yield conversion efficiencies in excess of 20%.

One of the interesting results in Table 1 is that we find that many of the effects can be almost entirely eliminated by proper cell design. Shadowing can be eliminated by using back-contact cells, V-groove reflective front-surface contacts or reflective V-groove cover glasses. Front-surface reflection effects can be reduced to nearly insignificant levels through the use of textured surfaces with antireflection coatings. Series resistance effects can be reduced to a negligible range even at extremely high concentrations through the use of unconventional cell structures; for instance, grid series resistance effects and emitter lateral voltage drops can be reduced to any level which is desired through the use of back-contact cell construction. Base series resistance effects can be reduced to negligible levels through a proper choice of base doping and device dimensions.

Contact recombination and surface recombination are somewhat more speculative in terms of the probability of eventually reducing these to negligible levels.

One technique for reducing contact recombination, of course, is to reduce the metal–semiconductor contact area as much as possible and, in fact, this has been done through the use of dot contacts and patterned back-surface contact areas. The effects of contact recombination have further been reduced by surrounding the metal contact area with a high–low junction region which has the effect of keeping minority carriers away from the very large recombination velocity associated with a metal–semiconductor contact. These high–low junctions become ineffective at very high illumination levels. However, it appears to be possible to reduce contact recombination to negligible levels by shrinking the contact areas to a small fraction of the cell area while also including a heterostructure between the silicon and the metal contact such that the majority carrier contact is maintained while minority carriers are prevented from reaching the metal–semiconductor contact. (Figure 1 shows a hypothetical heterostructure which would result in this behavior.)

The surface recombination velocity can be reduced in a number of ways, one of which involves the use of very clean processing procedures and oxidization techniques which yield very low surface state densities. This

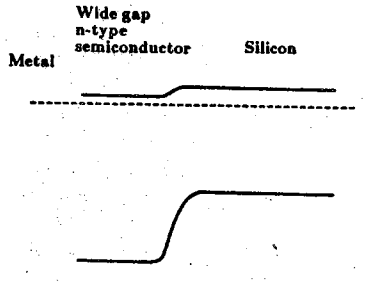

Fig. 1. Heterojunction isolation for metal semiconductor contacts.

technique is always effective and should be used even when other additional surface recombination reduction techniques are applied such as band-bending techniques which reduce the effective surface recombination velocity while keeping minority carriers away from the surface through the use of built-in fields.

It is very difficult to estimate the relative contributions of surface recombination, contact recombination and bulk recombination on today's high efficiency devices as the definitive experiments have not yet been performed.

Recent reports have indicated that ion-implanted hydrogen is able to reduce the surface state density at $Si-SiO_2$ interfaces to very low levels. If the capture cross section of these low density surface states is similar to that of higher density states, the surface recombination velocity for silicon solar cells would be sufficiently low that it would no longer be a dominant limiting factor.

This leaves us with the final entry in Table 1, that of bulk recombination. Two recombination mechanisms appear to dominate the performance of silicon solar cells: recombination through trapping energy levels in the band gap and Auger recombination. Auger recombination can be dominant in heavily doped regions such as the emitter at low intensities and throughout the device under high intensity operation near open circuit. Recombination through both of these mechanisms may be dramatically influenced by the presence of band gap narrowing, which appears to become important at carrier concentrations above 10^{17}. The effect of band gap narrowing is to increase the np product, and therefore the minority carrier concentration, over what it would be in the absence of band gap narrowing. This in turn leads to an increase in recombination. The primary effect of bulk recombination in the present high efficiency cells is observed in the open-circuit voltage V_{oc} and not in the short-circuit current. High efficiency cells already have collection efficiencies in excess of 90% and currently available technology indicates that collection efficiencies in excess of 96% are attainable with base dopings of current interest.

The reason that V_{oc} is most strongly affected by the recombination mechanisms available in the device is that under open-circuit conditions all carriers generated must recombine within the cell. The carrier concentration will build up to such a point that this occurs. Since the open-circuit voltage is logarithmically related to the excess carrier concentration, it is a measure of the total recombination. It should be noted that band gap narrowing in itself would have no detrimental effect on device performance if the various recombination mechanisms were reduced to negligible levels. It is only the enhancement of the minority carrier concentration and the consequent increase in bulk and surface recombination that causes the open-circuit voltage to be affected by band gap narrowing. The effects of band gap narrowing can be reduced through a reduction in the volume of heavily doped material in the cell.

It appears that the open-circuit voltage in today's devices is limited by recombination in the emitter which is increased by the presence of band gap

narrowing effects. Whether the actual recombination is occurring in the bulk of the emitter or at the SiO_2–Si interface is unknown. What is known is that the open-circuit voltage is 60 - 80 mV lower than it would be if band gap narrowing effects were not present.

3. Future high concentration silicon cells

For purposes of speculation, we have taken the view that all the effects listed in Table 1 except bulk recombination can be reduced to insignificant levels through proper cell design or device processing. For bulk recombination, there is reason to believe that there are fundamental limits in silicon which are not likely to be overcome. For lightly doped material it appears that the lifetime is limited to the range 500 - 1000 μs and is determined by recombination through trapping energy levels in the band gap. For heavily doped material, and for lightly doped material operating with very large excess carrier concentrations, the bulk recombination is dominated by Auger recombination.

Figure 2 presents the operating efficiency of an idealized silicon cell illuminated by an air mass 1.5 spectrum with concentration ratios ranging

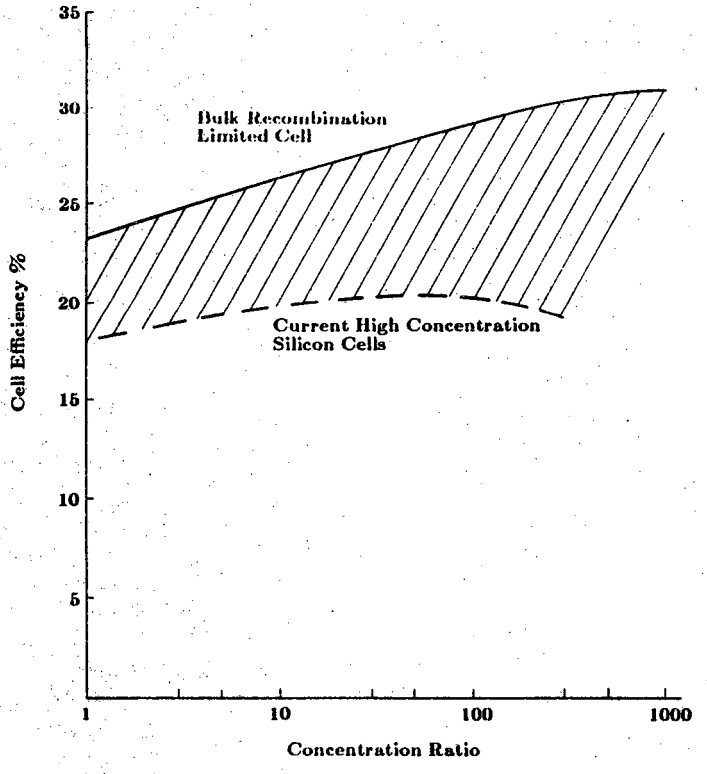

Fig. 2. Cell efficiency for an idealized silicon cell and present cells.

from 1 to 1000. This curve was obtained by utilizing a detailed computer code which takes into account Hall–Shockley–Read recombination, Auger recombination and mobility dependence on doping. The ideal device curve has been computed by optimizing the base doping and device thickness at each concentration ratio. For the idealized curve presented in Fig. 2, we have assumed that recombination at the surfaces and at the metal–semiconductor contacts have been eliminated and that band gap narrowing effects, grid series resistance, the lateral voltage drop in the emitter and reflection effects are negligible. While it is clearly very difficult to realize all these conditions simultaneously, it does appear that there are cell designs which will allow this situation to be approached. Also included in Fig. 2 is a curve showing the highest reported conversion efficiency at each concentration. The first feature that we note from Fig. 2 is that, contrary to popular belief, it appears that further significant increases in silicon solar cell performance are possible, particularly at high concentrations. The fall-off at high concentrations observed in the curve of present-day cells is due to a degradation in the fill factor. The origin of this, in these cells, appears to be a lateral voltage drop in the emitter.

Even at low concentrations, where the best present-day cell has an efficiency of 18%, there appears to be significant room for improvement. It appears that efficiencies of 23% should be obtainable. In order to achieve this high efficiency, however, considerable effort will need to be expended in the areas of surface passivation and contact isolation, as these two mechanisms will be dominant in those structures where other problems have been eliminated. Also, it should be noted that the optimized cells of Fig. 2 were obtained by using the assumption that the back surface of the cell was reflecting so that the light made two passes through the cell. One result of the optimization, however, was that all the cells have an optimum thickness in the range 50 - 60 μm. This is not true of present-day cells, which are fabricated with thicknesses of 250 μm and greater. Part of the reason for this is that present-day cells do not have surfaces which are as well passivated as is needed. They also suffer from recombination in the heavily doped regions and at the contacts. Until these high recombination regions are significantly improved, thick cell designs and lower conversion efficiencies will prevail.

4. A possible high efficiency concentrator cell

Figure 3 is a schematic diagram of one possible cell design which incorporates many of the features discussed above and which would yield efficiencies approaching those of the idealized curve of Fig. 2 if the very good surface passivation and contact isolation can be obtained. The cell features a reduced volume for the rectifying junction, reflecting grid structures which significantly reduce shadowing, textured surfaces with an antireflection coating, and a heterostructure contact. Also, the metallic contact areas are reduced to an absolute minimum. The grid lines are very narrow

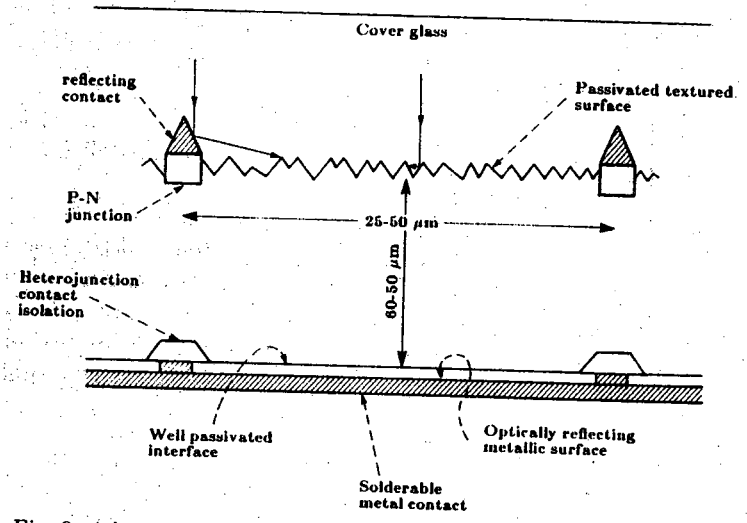

Fig. 3. A hypothetical high efficiency concentrator cell.

and closely spaced to minimize internal potential drops. The very thin base keeps the fill factor high, even at very large concentrations.

5. Conclusions

Much progress has been made in improving the efficiency of silicon concentrator cells, but significant room for improvement remains. Cells with efficiencies approaching 30%, at concentration ratios above 300, appear to be feasible but will require new structures, very careful processing and a better understanding of the factors controlling surface recombination, band gap narrowing and metal–semiconductor contacts than we now have.

APPENDIX D

This appendix contains a paper which was presented at the Seventeenth IEEE Photovoltaics Specialists Conference [7].

Reprinted from PROCEEDINGS OF THE SEVENTEENTH
IEEE PHOTOVOLTAIC SPECIALISTS CONFERENCE, May 1-4, 1984

TWO-DIMENSIONAL COMPUTER SIMULATION OF SINGLE CRYSTAL SILICON CONCENTRATOR CELLS

J. L. Gray and R. J. Schwartz
School of Electrical Engineering
Purdue University
West Lafayette, IN 47907

ABSTRACT

The factors which limit cell performance are examined and ultimate performance calculations are made for cells dominated entirely by recombination in the base. Maximum theoretical efficiencies of 23.4% at 1 AM1.5 sun, 32.0% at 100 suns, and 36.0% at 1000 suns are predicted for very thin ($\leq 75\,\mu m$) cells with lightly doped bases ($N \leq 1\times10^{15}\,cm^{-3}$). A two-dimensional simulation program, SCAP2D, is used to examine various cell geometries designed for high efficiency. These include the conventional, IBC, EMVJ, and grating cells. It is concluded that recombination at ideally ohmic metal contacts is the major factor limiting cell performance. Novel contact designs could increase the efficiencies of concentrator cells dramatically.

INTRODUCTION

The determination of the upper limit of efficiency of single crystal silicon solar cells is an important topic [1,2,3]. Knowing the ultimate efficiency and the factors limiting the efficiency of present and proposed cells will indicate where research efforts should be focused. In order to properly evaluate cell design, it is important to understand what the fundamental limitations to cell performance are. In a recent publication [3], the authors examined the mechanisms which limit device performance in an effort to determine which are fundamental limitations and which might be overcome. It was determined that the only fundamental limitation is recombination in the base; all other losses can probably be reduced to negligible levels by proper cell design and fabrication. A summary of these limiting factors is given in Table 1.

Table 1.
Factors Limiting Cell Performance

Limiting effect	Comments
Shadowing	Reduces J_{SC}. Can be eliminated with back contact cells or reduced with V-groove cover plates.
Series Resistance	Degrades fill factor. Resistive effects can be made insignificant with proper cell design.
Contact Recombination	V_{OC} is degraded. May be reduced by reducing contact area and through use of high-low junctions or heterojunctions.
Surface Recombination	V_{OC} reduced. Nonconventional cell designs require better surface passivation.
Bulk recombination	V_{OC} reduced. Recombination in the emitter and high-low junction can be reduced by keeping their volumes small wrt to total cell volume. Recombination in the base will control cell performance.

In this paper, several cell geometries will be compared. These include the conventional, IBC (Interdigitated Back Contact), EMVJ (Etched Multiple Vertical Junction), and grating cells. These cells will be simulated by a two-dimensional device simulation program, SCAP2D (Solar Cell Analysis Program in 2 Dimensions). SCAP2D solves Poisson's Equation and the two continuity equations simultaneously using finite differences to discretize the equations and Newton's Method to solve the resulting system of nonlinear equations. The program runs on a Cyber 205. A typical run simulating a device on a 55 by 36 finite difference mesh and computing 13 bias points requires less than five minutes of CPU time. Results will be shown for devices simulated under AM1.5 illumination at 1, 100, and 1000 suns. Basic cell parameters, such as device thickness, base doping, and junction depths, were determined beforehand and subsequently adapted to the various cell geometries which are to be simulated using the detailed simulation program, SCAP2D. The choice of these parameters is discussed in the next section.

DETERMINATION OF DESIGN PARAMETERS

Base Thickness and Doping

If we assume that recombination in the heavily doped regions, at the surfaces, and at the contacts can be held to negligible levels, and that ohmic losses in the emitter and contact grid can likewise be kept negligible; it is possible to estimate an optimum cell thickness and base doping density. For these assumptions, the current

can be approximated as the difference of two terms.

$$J = q\int_0^W G(x)dx - q\int_0^W R(x)dx \qquad (1)$$

The cell thickness is W, $G(x)$ is the generation rate, and $R(x)$ is the recombination rate.

The generation term can be computed as a function of device thickness once the spectrum and absorption coefficients are known. For our computations we have used an AM1.5 spectrum. In addition, we have assumed a double pass of the incident photons.

Let us now examine the recombination term. As long as the base is much shorter than a diffusion length, the excess carrier concentration in the base can be approximated as independent of position. Then, assuming quasi-neutrality (i.e. $\Delta p = \Delta n$), the recombination term can be written as follows.

$$q\int_0^W R(x)dx = \qquad (2)$$

$$qW(pn - n_{ie}^2)\left[A_n n + A_p p + \frac{1}{\tau_p(n+n_{ie}) + \tau_p(p+n_{ie})}\right]$$

An empirical expression for the effective intrinsic carrier concentration, n_{ie}, as a function of doping, as suggested by Slotboom and DeGraaff [4] has been used. Although this expression is based on measurements of p-type material, we have assumed the same expression holds for n-type silicon. For purposes of these calculations, n_{ie} has been assumed to be a function of doping only and not free carrier concentration. Measured values are used for the Auger recombination parameters, A_n and A_p [5]. A single level trap Shockley-Hall-Read mechanism is assumed with the trap at the intrinsic level. Since the base region is assumed to dominate recombination, the choice of the carrier lifetimes, τ_n and τ_p, will have the greatest impact on the results of these calculations. In order to model the degradation of carrier lifetime with doping, a modification of the empirical formula suggested by Fossum [6] is used.

$$\tau = \frac{500\,\mu\text{sec}}{1 + \frac{N}{7.1\times10^{15}}} \qquad (3)$$

N is the base doping density. The assumption here is that the best lifetimes obtainable in fabricated devices can be estimated from the above expression. Measurements of base lifetimes of devices fabricated at Sandia support this premise [7].

Since the excess carrier concentration is assumed to be uniform, the net carrier concentrations are easily computed in terms of the potential applied across the pn junction, V_j. Given the carrier concentrations, the contribution to the terminal voltage at the high-low (nn^+) junction, V_{hl}, can also be calculated. Assuming the current path is across the entire base thickness, the ohmic drop across the base is

$$V_b = \frac{JW}{qn\mu_n + qp\mu_p} \qquad (4)$$

An empirical expression for the mobilities as a function of doping as given by Arora, et. al. [8] is used. Carrier-carrier scattering is also included [9]. Since the carrier concentration is uniform, there are no Dember potentials.

At this point, we have expressions for the cell current, J, and the terminal voltage, V_t, in terms of only three parameters: V_j, the pn junction voltage, W, the cell thickness, and N, the base doping density.

$$J = J(V_j, W, N) \qquad (5)$$

$$V_t = V_j + V_{hl}(V_j, N) - V_b(V_j, W, N) \qquad (6)$$

For a given W and N, the current-voltage characteristic can be numerically computed, yielding the short-circuit current, open-circuit voltage, fill factor, and efficiency. In Figure 1, a contour plot of cell efficiency as a function of cell thickness and base doping is shown for 100 sun AM1.5 illumination. Note that the highest efficiencies are predicted for thin, lightly doped cells. The cross-hatched area is where the cell thickness exceeds half the ambipolar diffusion length, thereby violating the short base assumption.

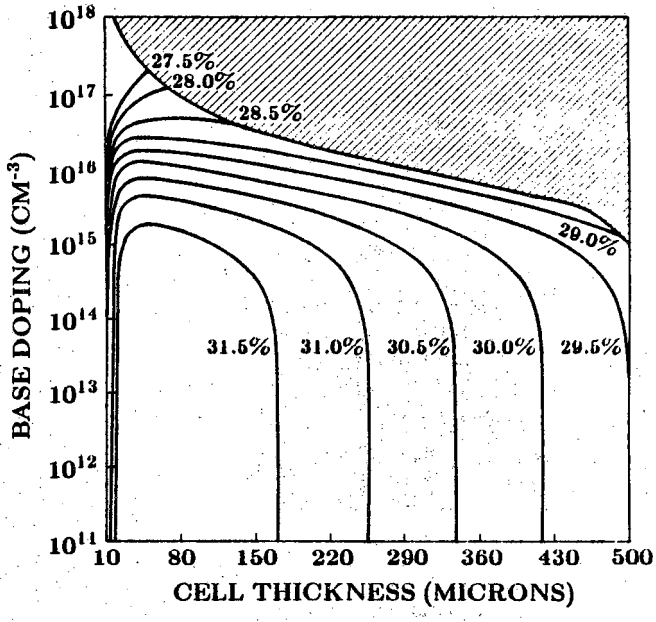

Figure 1.
Efficiency Contour Plot at 100 suns AM1.5

The basic solar cell parameters extracted from the maxima of the contour plots at 1, 100, and 1000 AM1.5 suns are tabulated in Table 2. At 1 sun there are two maxima. One is in the same region as for the higher solar concentrations, i.e. a thin, lightly doped cell; while the other, with a slightly higher efficiency, is for a somewhat thicker, moderately doped cell. The latter maximum fades as the solar concentration is increased. Since the regions of highest efficiency are broad, all SCAP2D simulations are performed for a cell thickness of 75 μm and a base doping of 5×10^{14} cm^{-3}.

Note that these predictions must be thought of only as ultimate limits, attainable only if the performance is entirely dominated by recombination losses in the base.

Table 2.
Maximum Performance Limits

	AM1.5 suns			
parameter	1	1	100	1000
$W\ (\mu m)$	30	130	50	75
$N\ (cm^{-3})$	1×10^{11}	3×10^{16}	1×10^{11}	1×10^{11}
$V_{OC}\ (V)$	0.802	0.687	0.996	1.021
$J_{SC}\ (A/cm^2)$	.0315	.0342	3.253	33.26
FF	0.772	0.840	0.820	0.882
$\eta\ (\%)$	23.4	23.7	32.0	36.0

Junction Depths and Doping

The doping and junction depth of the heavily doped regions can be roughly estimated as follows. In order to keep recombination in the heavily doped regions small, the junction depth, x_j must be much less than a minority carrier diffusion length, L_m, or $x_j = fL_m$ with $f \ll 1$. Assuming an ideal ohmic contact, the saturation current can be expressed as follows.

$$J_0 = \frac{qD_m n_{ie}^2}{N_M f L_m} \qquad (7)$$

D_m is the minority carrier diffusion coefficient and N_M is the doping density. Minimizing J_0 with respect to N_M, it is found that $N_M = 4\times10^{19}\ cm^{-3}$ and $x_j = 0.3\ \mu m$ are reasonable choices.

Surface Recombination

Recombination at the Si–SiO_2 interfaces is controlled by the the surface recombination velocities and by the net surface charge density [10]. A large surface charge density acts to to reduce the surface recombination rate. For the simulations presented in this paper, the surface recombination velocities are taken as $1000\ cm/sec$ with a surface charge density of $q\times10^{12}\ cm^{-2}$.

Metal Contacts

All metal contacts are assumed to be ideally ohmic for the simulation results presented here. In order to keep recombination losses at the contacts at a minimum, the contact areas have been selected to be consistent with 5 micron design rules. As will be shown, even this small metal coverage keeps the cells from reaching the highest predicted efficiencies.

SIMULATION RESULTS

All the devices were simulated using SCAP2D with the same basic cell parameters. The cell thickness and grid repeat distance were both taken to be $75\ \mu m$. The doping profiles in the diffused regions are taken as error function compliments with a surface concentration of $4\times10^{19}\ cm^{-3}$ and a junction depth of $0.3\ \mu m$. The grid width depends on cell geometry, but in most cases is $5\ \mu m$. The emitter and high-low junction volumes also depend on cell geometry, but are usually selected to be as small as possible in order to keep the recombination in these regions negligible. The surface recombination velocity at the Si–SiO_2 interface is taken as $1000\ cm/sec$ with a fixed surface charge density of $q\times10^{12}\ cm^{-2}$. The metal contacts are assumed to be ideally ohmic. A perfect anti-reflective layer has been assumed as well as a perfect back surface reflector.

Seven variations of the four basic cell geometries have been simulated under AM1.5 illumination at 100 suns. The illumination is incident from the bottom of the device cross-sections as shown in Figures 2 to 8. Normal incidence is also assumed. For the IBC, grating, and conventional cells the dimensions of the small metal contacts are $2.5\ \mu m$. The etched groove p^+ contacts of EMVJ-1 and EMVJ-2 are both $5\ \mu m$ deep, while for EMVJ-3 it is $25\ \mu m$ deep. The n^+ contact on EMVJ-1 is $2.5\ \mu m$ wide. The simulation results are tabulated in Table 3.

As might be expected, the performance of the four most comparable cells, the IBC, grating, conventional-1, and EMVJ-1, are very close. All these cells have small metal contacts, and except for the conventional-1 cell, small heavily doped regions. Since these cells were designed to flood the base with carriers, and since these cells are thin with respect to a diffusion length, it makes no difference, at least to first order, as to where the contacts are placed.

It is immediately apparent the the efficiency of these devices is nowhere near the predicted theoretical maximum of 32%. Although we are achieving almost perfect 100% collection efficiency and the fill factors are close to the predicted 0.82, the open-circuit voltages are far below the predicted maximums. The source of this difficulty is immediately apparent when the sources of recombination are examined at V_{OC}. Under open-circuit conditions, all the carriers generated in the device must also recombine there. In order to achieve the high open-circuit voltages predicted, two conditions must be satisfied. The base recombination parameters must be as good as possible, meaning that carrier lifetimes must be long, and recombination in the base must be the dominate recombination mechanism. Although we have assumed the first

Table 3.
SCAP2D Simulation Results at 100 suns AM1.5

Cell	$V_{OC}\ (V)$	$J_{SC}\ (A/cm^2)$	FF	$\eta\ (\%)$	$\eta_{active}\ (\%)$	$\eta_c\ (\%)$
IBC	.759	3.22	.804	23.6	23.6	96.7
grating	.758	3.16	.803	23.2	24.0	98.4
conventional-1	.754	3.21	.818	23.8	24.6	99.9
conventional-2	.711	3.21	.784	21.5	22.2	99.9
EMVJ-1	.741	3.17	.799	22.6	23.4	98.6
EMVJ-2	.704	2.50	.740	15.7	16.2	77.7
EMVJ-3	.684	2.97	.779	19.1	19.7	92.2

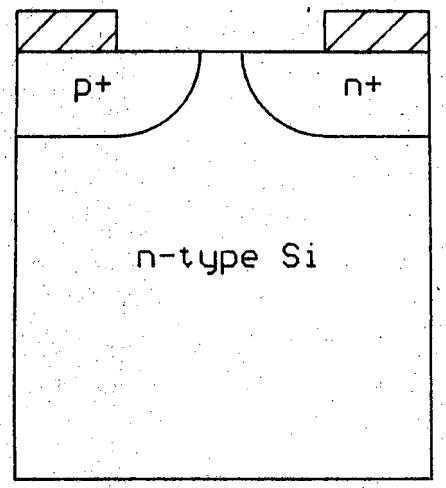

Figure 2.
IBC Cell

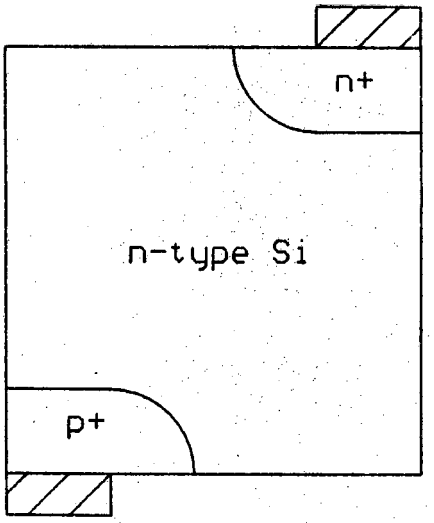

Figure 3.
Grating Cell

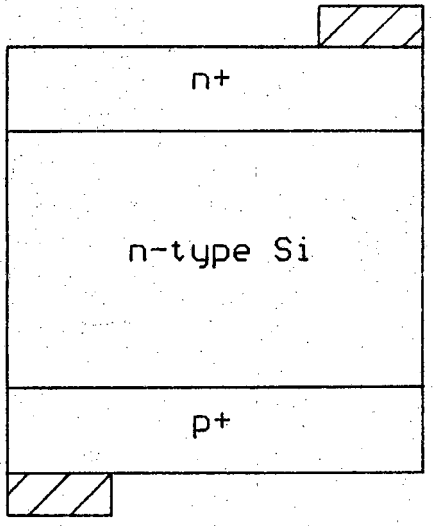

Figure 4.
Conventional-1 Cell

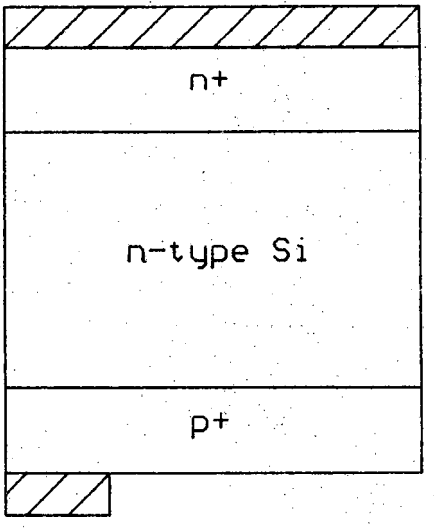

Figure 5.
Conventional-2 Cell

condition, the second is clearly not satisfied for these devices. In Table 4, the relative contribution to the total recombination from the various sources for the IBC cell are tabulated. Nearly 90% of the recombination occurs at the metal contacts. A simple 'back of the envelope' calculation shows that if recombination at the metal contact could be eliminated and was redistributed proportionately among the remaining sources of recombination (column 3 of Table 4), V_{OC} could possibly be increased by 0.115 V. If the the fill factor remained unchanged, this would boost the efficiency to 27.2%. Although eliminating the metal contacts as a source of recombination will increase the relative importance of recombination in the base, it will still not be the dominate mechanism for the device modeled here. Surface recombination will dominate. Improving the $Si-SiO_2$ interface passivation will not, however, significantly help until recombination at the metal contacts is controlled.

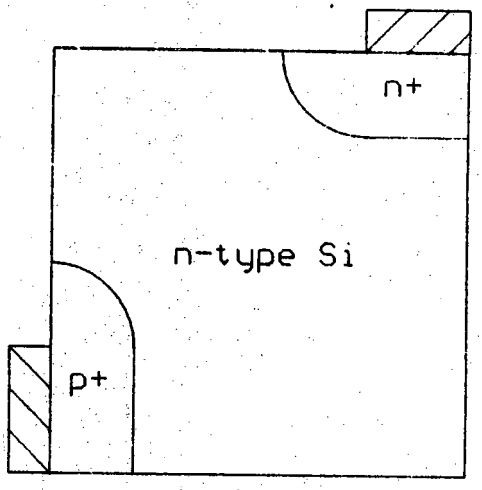

Figure 6.
EMVJ-1 Cell

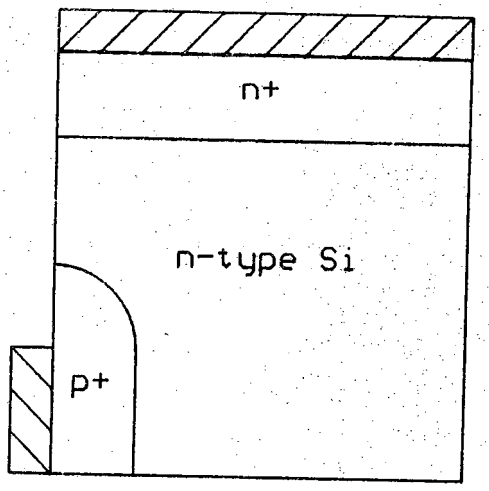

Figure 7.
EMVJ-2 Cell

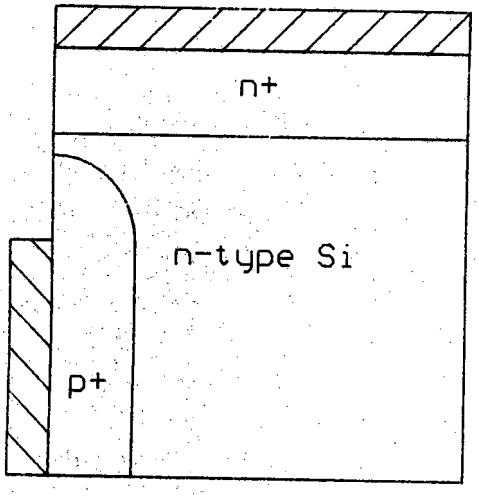

Figure 8.
EMVJ-3 Cell

Table 4.
Relative Contribution to Recombination at V_{OC} for an IBC Cell at 100 suns

Source	relative contribution %	relative contribution (metal zero)
base	1.6	14.4
emitter	0.1	0.9
high-low	0.1	0.9
SiO_2 interfaces	9.3	83.8
metal contacts	88.9	none

The difference in performance between the two conventional cells is completely attributable to the difference in metal coverage. The open-circuit voltage is severely degraded by the total back metal coverage.

The clear superiority of EMVJ-1 over the other EMVJ cells is again due almost entirely to the difference in metal coverage. The lower the contact area, the greater the open-circuit voltage. It is interesting to note that the collection efficiency of EMVJ-2, with a shallow etched groove, is much less than that of EMVJ-3, with the deep etched groove. The high-low junction is not efficient at containing the excess carriers in the base and many recombine at the back contact rather than be collected since the high-low junction area is much larger than the emitter junction area. Increasing the emitter junction area (EMVJ-3) increases the collection efficiency since the carriers have a greater chance of 'seeing' the collecting junction before recombining.

Simulation results for the four 'best' devices at 1 and 1000 suns are shown in Tables 5 and 6, respectively. At 1 sun, the efficiencies are much closer to the predicted maximum and are close to the values reported in the best cells made at present. Although recombination at the metal contacts still dominates, its relative contribution is not as great as that seen at higher intensities. At 1000 suns, the IBC cell, and, to a lesser extent, the grating and EMVJ cells, are beginning to show the effects of loss of surface passivation [10]. This is seen in the reduced collection efficiencies. As before, recombination at the metal contacts keeps the open-circuit voltage, and therefore the efficiency of these cells is far below the predicted maximum.

Table 5.
SCAP2D Simulation Results at 1 sun AM1.5

Cell	V_{OC} (V)	J_{SC} (mA/cm^2)	FF	η (%)	η_{active} (%)	η_c (%)
IBC	.637	32.8	.821	20.6	20.6	98.5
grating	.635	31.8	.820	19.9	20.6	98.8
conventional-1	.631	32.1	.822	20.0	20.7	99.9
EMVJ-1	.619	31.7	.821	19.4	20.1	98.7

Table 6.
SCAP2D Simulation Results at 1000 suns AM1.5

Cell	V_{OC} (V)	J_{SC} (A/cm^2)	FF	η (%)	η_{active} (%)	η_c (%)
IBC	.817	28.5	.751	21.0	21.0	85.7
grating	.820	30.6	.753	22.7	23.5	95.2
conventional-1	.814	32.0	.714	22.4	23.2	99.7
EMVJ-1	.802	31.0	.744	22.3	23.0	96.2

CONCLUSIONS

Very high efficiencies have been predicted, 32% at 100 suns, for devices which are dominated by recombination in the base, and where the base lifetimes are as long as possible. Design parameters were derived which were expected to approach this condition. However, two-dimensional computer simulations of cells geometries utilizing these parameters show that even for very small metal contact coverage, recombination at the metal contacts completely dominates under open-circuit conditions. The result of this domination is to severely reduce the open-circuit voltage and cell efficiency.

In order to realize significant improvement in cell efficiency, some type of novel contact, which is ohmic to majority carriers, but is also a good minority carrier mirror, must be developed. Some type of heterostructure, with contact made to a wide gap material deposited on the silicon, may offer a solution [3]. Once recombination at the metal contacts is controlled, surface passivation will increase in importance. If these problems can be solved, significant improvements in cell performance will be realized.

ACKNOWLEDGMENTS

This work was supported by the United States Department of Energy through Sandia National Laboratories, document number 52-5675. The authors would also like to thank Dr. D. Arvizu of Sandia National Laboratories for helpful technical discussions.

REFERENCES

[1] Martin Wolf, IEEE Trans. Electron Devices, ED-27(4),pp. 751-760 (April 1980)
[2] H. J. Hovel, Semiconductors and Semimetals, Vol. 11 (Solar Cells), pp. 72-80, Academic Press, Inc., New York, N.Y. (1975)
[3] R. J. Schwartz and J. L. Gray, to be published in Solar Cells
[4] J. W. Slotboom and H. C. DeGraaff, Solid-State Electron., Vol. 24, pp. 857-862, (1976)
[5] J. Dziewior and W. Schmid, Appl. Phys. Lett., Vol. 31, pp. 346-348 (1977)
[6] J. G. Fossom, Solid-State Electron., Vol. 19, pp. 269-277 (1976)
[7] B. H. Rose and H. T. Weaver, J. Appl. Phys., Vol. 54(1), (Jan. 1983)
[8] N. D. Arora, J. R. Hauser, and D. J. Roulston, IEEE Trans. Electron Devices, ED-29(2), pp. 292-295 (Feb. 1982)
[9] J. M. Dorkel and Ph. Leturcq, Solid-State Electron., Vol. 24(9), pp. 821-825 (1981)
[10] J. L. Gray, R. J. Schwartz, and R. D. Nasby, Sixteenth IEEE PVSC, pp. 437-441, (1982)

APPENDIX E

This appendix contains a paper presented at the High-Efficiency Crystalline Silicon Solar Cell Research Forum in Phoenix, Arizona in July 1984 [8].

Current Status of One and Two-Dimensional Numerical Models: Successes and Limitations

by R. J. Schwartz, J. L. Gray, and M. S. Lundstrom
Purdue University
School of Electrical Engineering
West Lafayette, IN 47907

Abstract

The capabilities of one and two-dimensional numerical solar cell modeling programs (SCAP1D and SCAP2D) are described. The occasions when a two-dimensional model is required are discussed. The application of the models to design, analysis, and prediction are presented along with a discussion of problem areas for solar cell modeling.

Introduction

Accurate numerical models for single crystal silicon solar cells have proven to be very reliable in the simulation of the performance of these cells. These models have proven to be extremely useful in: the interpretation of experimental measurements; the identification of processes which limit cell performance; the prediction of benefits which will result from design and materials changes; the comparison of various cell designs; and the prediction of efficiencies which may eventually be obtained in silicon solar cells as various technological barriers are overcome.

The capabilities of a one-dimensional (SCAP1D) and a two-dimensional model (SCAP2D) are described and examples of their use for each of the above purposes are given.[1-3] It will be shown that there are circumstances under which cells which appear to be one-dimensional require a two-dimensional model to properly simulate their behavior.

As cells become more efficient the requirements on the accuracy of the physics used in the model become more stringent. Effects which are of little significance in poor or moderately good cells can take on major significance in high efficiency cells. A number of problem areas which are of concern in the modeling of high efficiency cells are discussed. These include heavy doping effects, metal-semiconductor boundary conditions, minority carrier mobilities, high injection lifetimes, and carrier-carrier scattering. Each of these may have a major impact on the performance of the cell under certain operating conditions.

The Model

Physical Effects of Importance

One of the major advantages of a numerical model is that it affords one the opportunity to include the very large number of physical effects which may be acting simultaneously within a solar cell. The complexity of the phenomena and their interactions with each other preclude analytic solutions in anything except highly idealized situations, which are not indicative of actual cells or operating conditions. An attempt has been made in the formulation of SCAP1D and SCAP2D to include as many of the physical effects which are known to influence cell performance as possible and to do this in a manner which represents our

present knowledge of these effects. One of the goals in writing these codes was to have them be sufficiently accurate in their representations so that they could be used in a predictive mode. This is possible only if all of the pertinent physical effects are included.

In those cases where the physics is questionable, we have attempted to include options which allow one to choose between various models. For example, in the case of heavy doping effects, one is able to choose between the models of Slotboom, Lanyon-Tuft, and Mahan, or to supply a subroutine of one's own choosing.

We have attempted to choose materials parameters which in our estimation are the most reliable. These materials parameters are used as default values. The user can easily change these parameters to values that he views as more reasonable.

The following physical effects are included in the codes: hole and electron mobilities, including their doping and temperature dependencies; heavy doping effects, using the formulation of Lundstrom, Schwartz, and Gray; absorption coefficients, including their temperature dependence; recombination, including Auger, Hall-Shockley-Read, and surface recombination. Surface recombination is handled through the specification of the surface recombination velocity. In the case of SCAP2D, the effects of surface potentials are also included.

Semiconductor Equations

The programs perform a full simultaneous numerical solution of the two continuity equations and Poisson's equation subject to the boundary conditions appropriate to one and two-dimensional cells. The equations are formulated as shown in equations 1-3.

$$\nabla^2 v = -\frac{q}{\epsilon}(p - n + N_D - N_A), \tag{1}$$

$$\nabla \cdot \mathbf{J}_p = q(G - R), \tag{2}$$

$$\nabla \cdot \mathbf{J}_n = q(R - G). \tag{3}$$

The generation term in equations 2 and 3 are given by

$$G(x) = \int_0^\infty \Phi \alpha e^{-\alpha x} d\lambda \tag{4}$$

and the recombination term is given by equations 5, 6 and 7.

$$R = (pn - n_{ie}^2)\left[A_n n + A_p p + \frac{1}{\tau_n(p + p_1) + \tau_p(n + n_1)}\right] \tag{5}$$

$$\tau_p = \frac{\tau_{po}}{1 + \dfrac{(N_D + N_A)}{N_c}} \tag{6}$$

$$\tau_n = \frac{\tau_{no}}{1 + \dfrac{(N_D + N_A)}{N_c}} \tag{7}$$

The hole and electron current densities which appear in equations 2 and 3 are given by

$$J_p = -q\mu_p p \nabla v_p - kT\mu_p \nabla p \tag{8}$$

$$J_n = -q\mu_n n \nabla v_n + kT\mu_n \nabla n \tag{9}$$

$$v_p = v - (1-\gamma)\frac{\Delta_G}{q} \tag{10}$$

$$v_n = v + \gamma\frac{\Delta_G}{q} . \tag{11}$$

where v_p and v_n are the effective potentials defined in equations 10 and 11 and Δ_G and γ are parameters which account for variations in the band structure, such as density of states and band gap, and account for Fermi-Dirac statistics.

No low injection assumptions are made. The equations are solved from contact to contact with appropriate boundary conditions so that the solutions are valid for all ranges of operation and include minority and majority carrier flow. The latter places some restrictions on the CPU word size required for solution.

These codes have been extensively tested for accuracy by comparing the results of their predictions with experimental results obtained on very carefully and extensively characterized cells for a wide range of cell designs and operating conditions. The agreement has been such that a high degree of confidence has been developed in results computed using these codes.

Code Description

Figure 1 is a block diagram of the structure of SCAP1D and SCAP2D. The operator must supply information about the materials parameters, a description of the device to be analyzed, the type of analysis which he wishes to perform, and the spectrum, if appropriate. He also can, if he wishes, control some of the details of the numerical solution; the amount of information supplied while the program is converging to an answer and how the output information will be stored or displayed.

The results of the computation are presented in printed summary form and the detailed results of the calculation are stored on magnetic tape. A separate plotting routine is used to access the information on tape and to display the appropriate parameters. The plotting capability is one of the most valuable features of the code, in that it allows one to effectively have a microscopic view of most of the parameters of interest in the interior of the cell under operating conditions. We will show some of the available graphical output as we discuss the capabilities of the code. Table I shows the input control offered to the operator. In every case default parameters are specified if the operator chooses not to supply a parameter.

Table II contains a listing of plots which are available through the plotting program. In this case the operator specifies the type of plot which is required and the region of the cell for which he desires that plot. Most of the figures which follow were obtained directly from this plotting routine.

In addition to the reliability of the output, the utility of codes of this type will depend on their ease of use and efficiency of computation. For example, in a design mode, it is

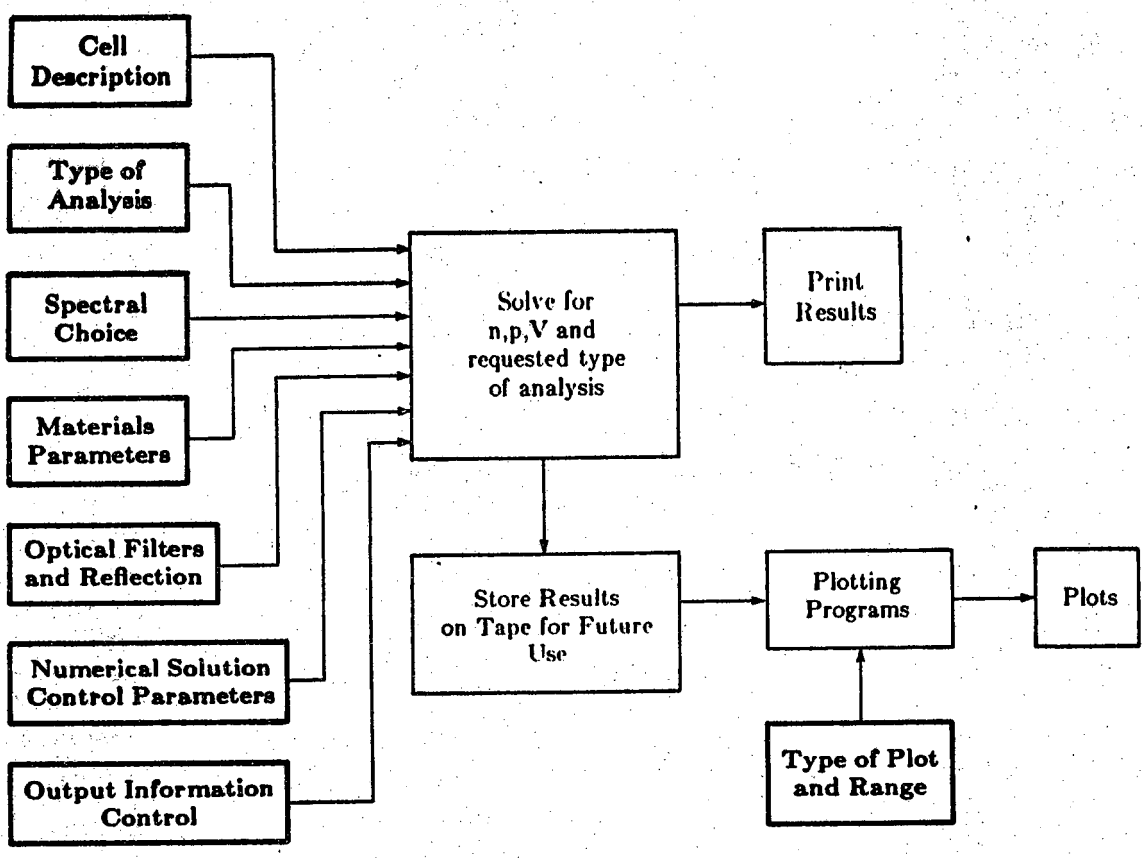

Figure 1 Block Diagram of the Structure of SCAP1D and SCAP2D

Table I - Input Parameters

Device Description
- Doping Profiles
  - Step junction
  - Erfc (N_s,x_j)
  - Experimental Profile
  - SUPREM II
- Dimensions

Materials Parameters
- Lifetime (τ and energy)
- Surface Recombination
- Auger
- Bandgap narrowing
  - Slotboom
  - Mahan
  - Lanyon-Tuft
  - User supplied

Spectral Choices
- AM 0
- AM 1.0
- AM 1.5 direct & global
- Monochromatic
- Uniform generation
- User supplied

Optical Filters & Reflection
- Filter (Ge, Si, SiO_2, GaAs)
- Back surface reflector

Types of Analysis
- Dark I-V
- Illuminated I-V
- Solar Cell
- Spectral Response

Table II - Plotting Options

Carrier concentration	Hole current density and components
Hole and electron current densities	Electron current density and components
Change in potential (from equilibrium)	Mobility
Doping density	Lifetime
Energy band diagram	Ratio of n_{ie}/n_{io}
Electric field	Potential
Hole and electron quasi-electric fields	Recombination rate
Effective fields (electric plus quasi-electric) for holes and electrons	Charge density
	Excess carrier concentration
Optical generation	

advantageous to be able to make multiple runs in a reasonable length of time and at reasonable cost. While SCAP1D can be run effectively on nearly any mainframe computer (a typical run on a CDC 6600 requires 100-300 CPU seconds), SCAP2D requires a very fast machine with a large amount of actual or virtual memory. On a Cyber 205, 300 CPU seconds are required for a typical run.

Situations Requiring Two-Dimensional Analysis

In many situations a one-dimensional simulation is quite adequate and there is no need to use the more complex and expensive two-dimensional simulation. On the other hand, there are a number of situations which only a two-dimensional simulation will suffice.

Some of the situations which require two-dimensional analysis are quite obvious, while others appear to be one-dimensional in nature, but, in fact, require a two-dimensional solution for proper description of the cell performance. Most of the cell structures which have been proposed as high efficiency silicon cells fall into the obviously two-dimensional analysis category. Among these structures are the Interdigitated Back Contact cell, the Vertical Multi-Junction cell, the Etched Multiple Vertical Junction cell, the Polka Dot cell, and the Grating cell. As an example of the use of SCAP2D in the analysis of these two-dimensional cells, we show figures 2 through 4 for an IBC cell. In Figure 2 we show the total short circuit current flow under one sun-conditions. In Figures 3 and 4 we show the majority and minority carrier flows for this same cell operating under the same condition.

Less obvious applications of the two-dimensional code are shown in Figures 5 through 6 in which a conventional solar cell has been analyzed. In Figure 5 we show the potential distribution along the emitter from a point half way between the grid lines up to the grid lines under open circuit conditions. This figure illustrates that there is a lateral voltage drop along the emitter, even under open circuit conditions, as a result of the current which is injected in the vicinity of the grid line. Figure 6 shows the circulating currents which exists in the vicinity of the grid line.

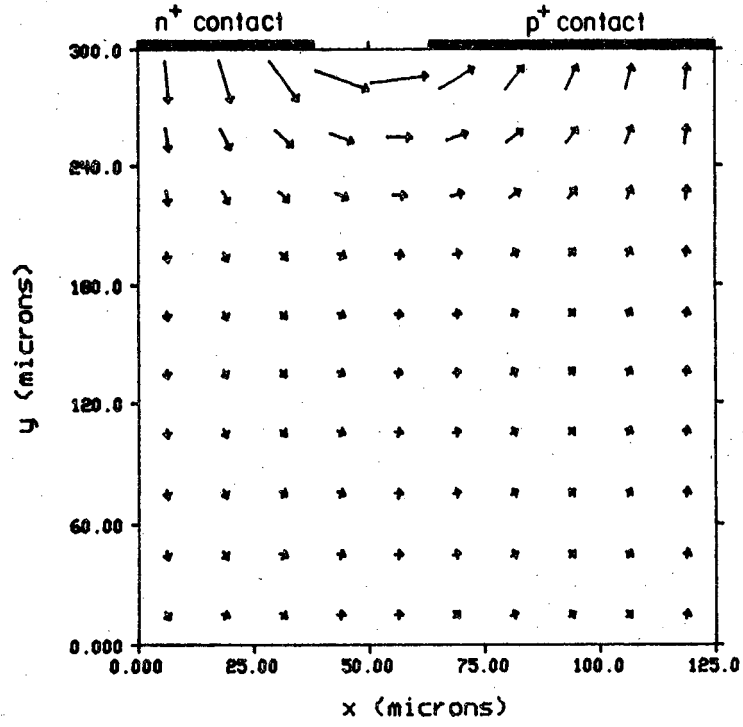

Figure 2 Total Short Circuit Current for an IBC Cell 1 Sun AM1.0

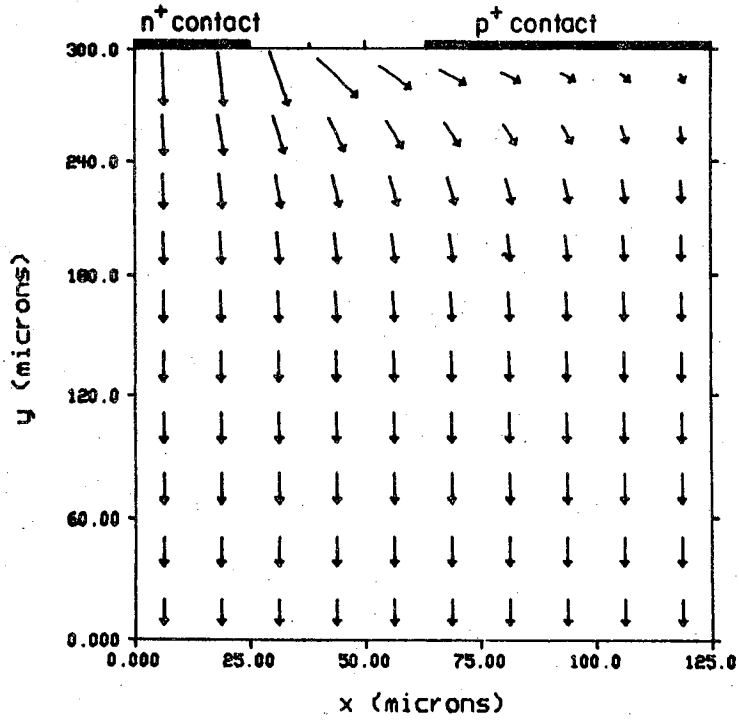

Figure 3 Majority Carrier Current Flow for the Cell of Figure 2

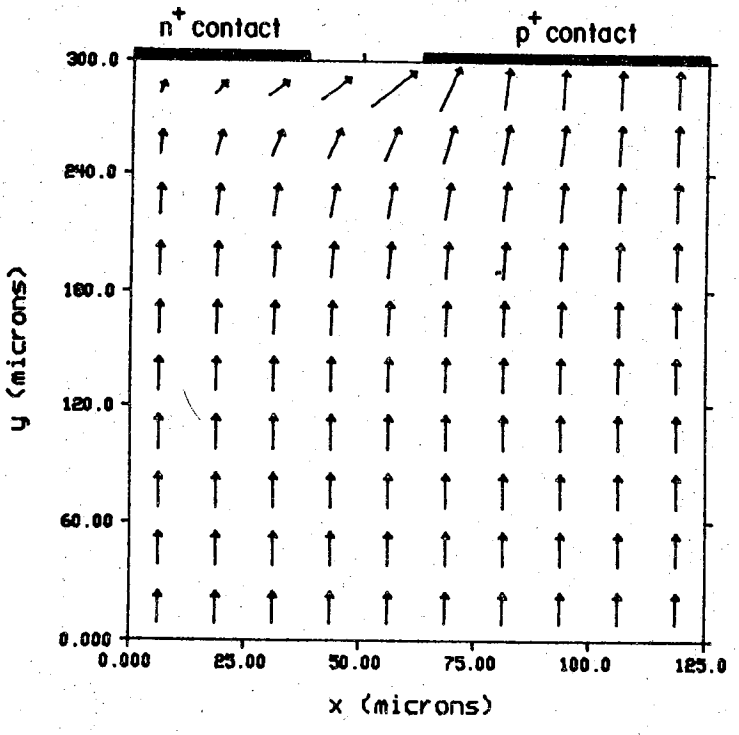

Figure 4 Minority Carrier Current Flow for the Cell of Figure 2

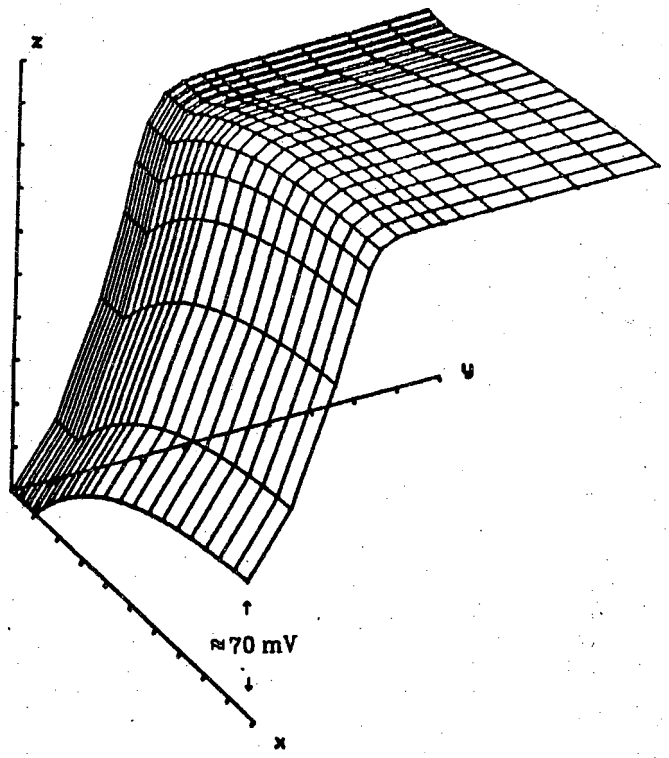

Figure 5 Potential Distribution in the Emitter of a Conventional Solar Cell Operating at 400 suns.

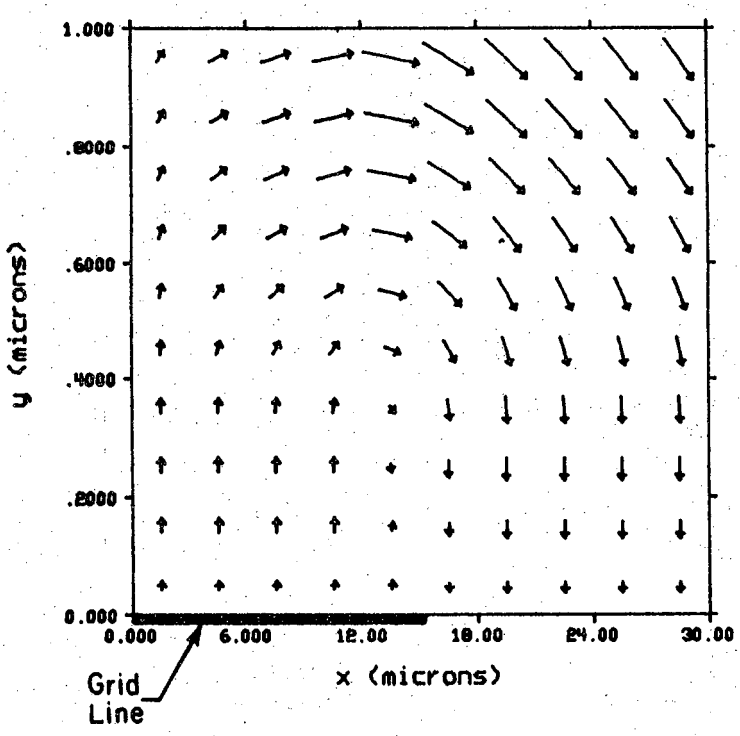

Figure 6 Circulating Current in the Vicinity of a Grid Line for a Conventional Solar Cell

An even less obvious problem with one-dimensional simulation occurs when one tries to properly model the front surface of a conventional cell. This surface is composed of a SiO_2-Si interface and a metal-semiconductor contact. In a one-dimensional simulation, one is forced to aggregate the two effects with some equivalent front surface recombination velocity, S_F. Figure 7 illustrates the difficulty with this approach. Under short-circuit conditions the proper value of S_F is equal to the surface recombination velocity of the SiO_2-Si interface. However, near open circuit conditions, the proper value of S_F may be 3 to 4 orders of magnitude larger. This is a result of the fact that the metal semiconductor contact may be a very effective recombination site for minority carriers. It is particularly important as the operating voltage of the cell increases. For proper operation of a one-dimensional code, the front surface recombination velocity should be a function of operating condition. The two-dimensional code does not have this problem, since the surface recombination velocity at the SiO_2-Si interface and the metal semiconductor interface are specified separately, and the recombination along the entire surface is properly accounted for under all operating conditions.

At high operating conditions, such as are found in concentrator solar cells, even the conventional cell behaves in a two-dimensional fashion and must be modeled using the two-dimensional code. Minority carrier current flow for a conventional cell operating at 800 suns is shown in Figure 8. If this cell is modeled using the one-dimensional code under these operating conditions, serious errors are encountered in the computation of the fill factor which can not be compensated for by including an external series resistance in the model, as the effect is nonlinear.

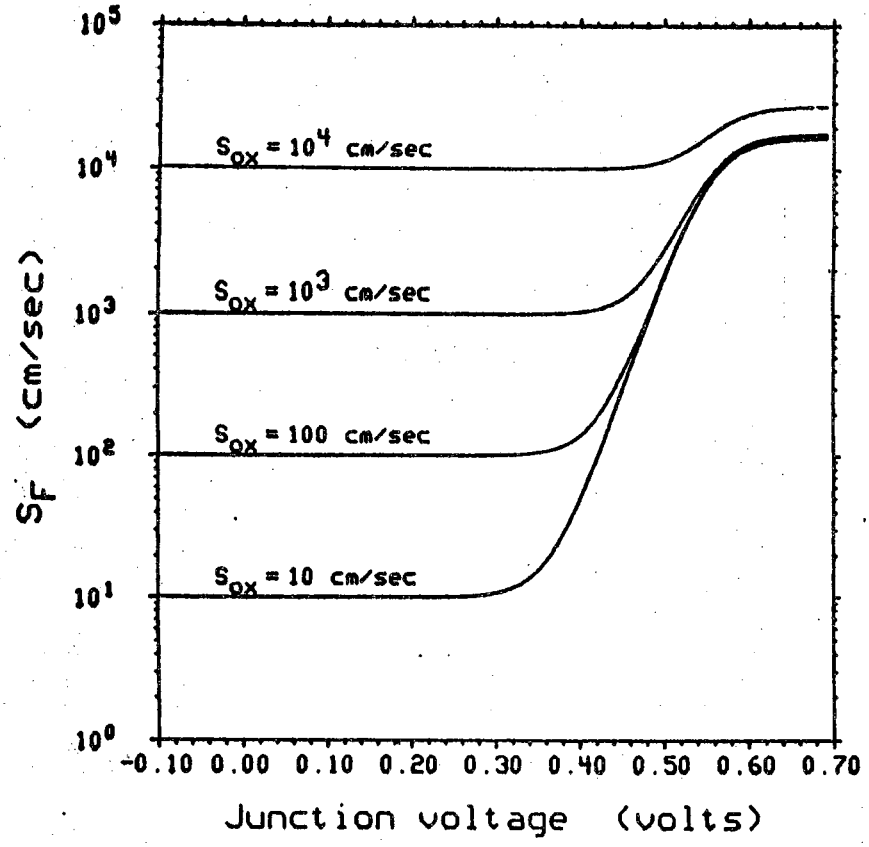

Figure 7 Effective Surface Recombination Velocity as a Function of Operating Voltage and the SiO_2-Si Surface Recombination Velocity

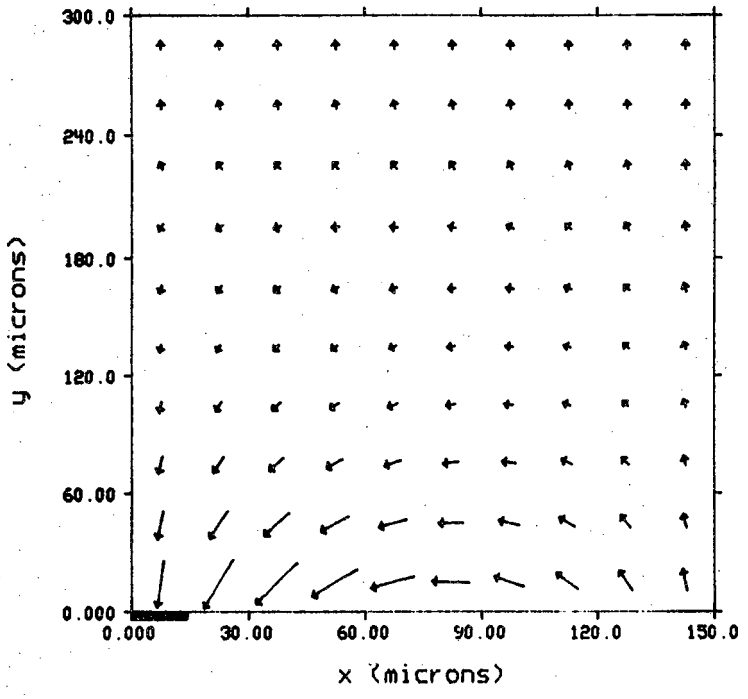

Figure 8 Minority Carrier Current Flow for a Conventional Solar Cell Operating at 800 Suns (V=.600 volts J=21.6 amp/cm^2)

Modes of Utilization

As we mentioned previously, a carefully prepared solar cell model is useful in a number of modes. In this section we will discuss the use of SCAP1D and SCAP2D as a design tool, a sensitivity analysis tool, an aid in the analysis of experimental data, an aid in the provision of insight into the operation of the cell, and, finally, as a predictive tool for the comparison of proposed cell designs and as a means of projecting performance as various technological barriers are removed. For the sake of continuity, we have chosen to use the Sandia high concentration cell operating at 1 sun as a base line design. This is a cell which has exhibited 18% conversion efficiency at one sun, and 20% conversion efficiency in the 50-100 sun range for an AM 1.0 spectrum.

Design

As a simple example we show, in Table III, the effects of variations in the base doping about the present design doping of 2.29×10^{16}, on the performance of this cell. We see that the present base doping is nearly optimum for the design parameters used in the other parts of the cell.

Table III

Solar Cell Performance Dependence on Base Doping
AM 1.0 (one sun)

Base Doping cm^{-3}	V_{oc} volts	J_{sc} ma/cm^2	F.F.	Efficiency %
5×10^{15}	.634	35.1	.828	18.35
1×10^{16}	.640	34.8	.833	18.46
2.29×10^{16}	.649	34.4	.836	18.55
1×10^{17}	.656	33.3	.838	18.21
5×10^{17}	.650	30.2	.836	16.37

Sensitivity Analysis

By utilizing a computer code such as SUPREM to simulate fabrication conditions one can model the sensitivity of device performance to fabrication parameters. Here, as an extreme case, we examine the effects of changes in the emitter doping profile on cell performance. The Sandia cell was simulated using the two emitter profiles shown in Figure 9. In Table IV, a comparison of these simulations is shown. Note that the erfc emitter profile simulation predicts a higher V_{oc}. This is due to the lower net recombination in the emitter as compared to the SUPREM II emitter profile simulation, as shown in Figure 10. Recombination is higher in the SUPREM II emitter because the doping is higher over most of the emitter volume, and therefore Auger recombination is correspondingly higher also.

If the results of a process simulation program such as SUPREM are coupled with SCAP1D or SCAP2D as shown above the sensitivity of the cell to process variations can be readily established.

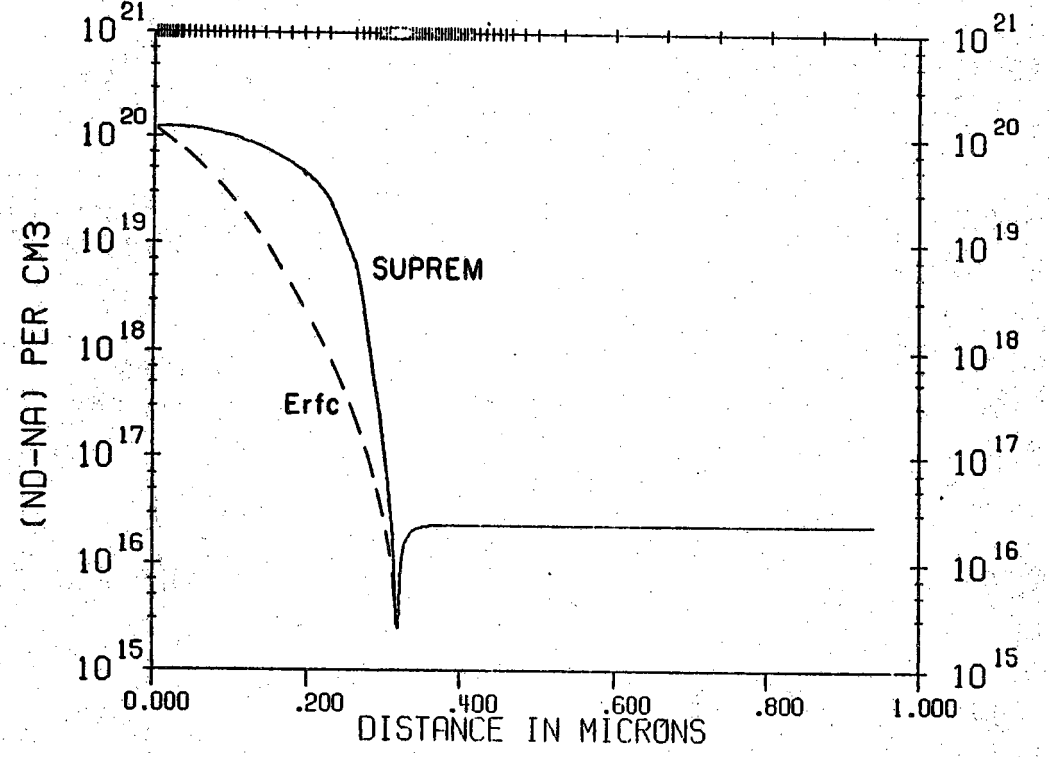

Figure 9 Emitter Doping Profiles as Determined by SUPREM II and Complimentary Error Function

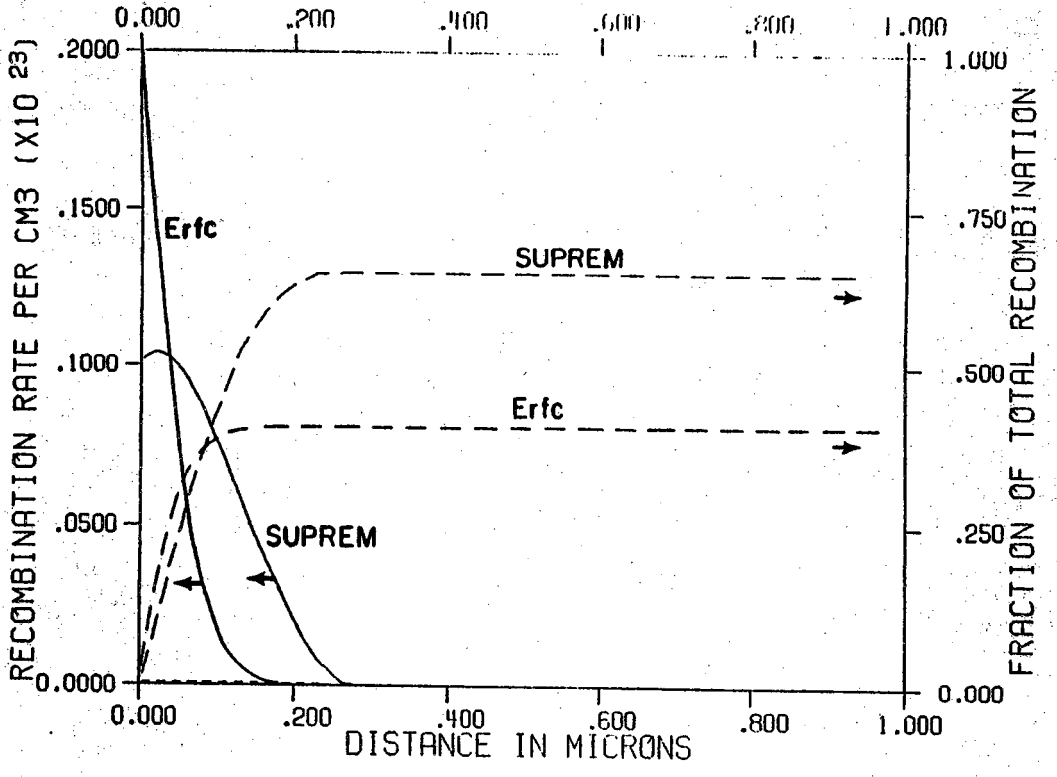

Figure 10 Emitter Recombination for the Two Doping Profiles Shown in Figure 9

Table IV

Dependence of cell performance on emitter doping profile
AM 1.0 (one sun)

Type of Profile	V_{oc} volts	J_{sc} ma/cm^2	FF	Efficiency %
Erfc	.648	34.3	.836	18.6
SUPREM II	.632	33.9	.833	17.75

Analysis

It is possible, by adjusting the parameters entered into the code, to obtain a fit between the model generated results and experimental dark I-V, solar cell, and spectral response curves. If this fit can be obtained for a single set of parameters, then one has a reasonable expectation that these are the correct parameters describing this device.

Insight

With the ability to observe most of the parameters of interest as a function of position and operating conditions anywhere within the cell, it is possible to achieve a great deal of insight into the limiting factors on any cell design. Examination of the model for the 20% Sandia cell very quickly establishes that the cell appears to be emitter limited, and, in fact, that further efforts in improving the performance of the cell should be devoted to reduction of the metal-semiconductor contact recombination and in reducing the volume of the heavily doped emitter.

Prediction

Potentially one of the most valuable, and also one of the most risky, uses of the numerical models is as a predictive tool. The models have already been shown to be quite reliable in comparing the relative merits of different cell designs. One particularly attractive way to utilize the code is to use it to identify limiting phenomenon in a particular cell design and then to remove that limitation and observe the effect on cell performance. In this fashion, one can predict benefits which will accrue through various advances in technology, and, in fact, can make some reasonable estimates of the ultimate performance of silicon single crystal solar cells. This latter use of the code is particularly risky since as the performance of the cell improves, physical effects which may have been insignificant in their effect on cell performance before, may suddenly become the dominant limitation.

Problem Areas

There are a number of areas in which there is concern about existing solar cell models either because the physics is not well understood, available data is thought to be unreliable, or because the effect has not been include in the model. These areas of concern are discussed below.

Heavy Doping Effects

There is a controversy over the origins and magnitude of heavy doping effects. There is a great deal of scatter in the measured effective band gap narrowing, particularly in the very heavily doped samples where we have our major concern. In order to alleviate this situation somewhat, we have provided the operator with the option to choose between most of the popular band gap narrowing models. This remains an area of major concern and is probably the least reliable area in the modeling of silicon solar cells.

Auger Recombination

Some uncertainty exists about the reliability of published Auger coefficients. At least two groups (Sandia and General Electric) have indicated that published Auger coefficients may be too large.

Minority Carrier Mobility

Reliable measurements of minority carrier mobility do not exist. Various authors have proposed that the minority carrier mobility is larger, smaller, and the same as the majority carrier mobilities of the same type carrier. As a consequence, SCAP1D and SCAP2D assume that the minority carrier mobilities for electrons are the same as they would be if electrons were majority carriers. A similar assumption is made for holes.

Metal-Semiconductor Contacts

In well designed high efficiency solar cells, the metal semiconductor contact limits the open-circuit voltage. The removal of this high dark current source, through the use of tunneling contacts or through the reduction of the metal-semiconductor contact area, has already demonstrated a significant improvement in open-circuit voltage. Further advances in this area may well employ heterojunction structures in addition to the present tunneling structures. SCAP1D and SCAP2D allow for specification of a finite minority carrier surface recombination velocity to model this effect.

Doping Profiles

We have already seen that device performance can be a strong function of the shape of the emitter doping profile. SCAP1D and SCAP2D allow for the use of a complimentary error function, a computed profile based on the Fair diffusion model for phosphorus, doping profiles obtained from a process simulation program such as SUPREM, or experimental data. The use of data from SIMS measurements has the problem that it includes the total impurity concentration not just the electrically active dopants. If any precipitation is present in the highly doped region, SIMS will overestimate the amount of active dopant. Spreading resistance measurements are a measure of the free carrier concentration. Near the depletion region this can lead to significant errors in the doping profile if the spreading resistance profile is interpretated as being the same as the doping profile.

Spectral Response

Spectral response measurements are particularly useful for obtaining information about the base lifetime and the surface recombination velocity. However, some difficulty is experienced in matching long wavelength response with computed response. This difficulty has been traced to the fact that small changes in device temperature can lead to large changes in the long wavelength response as a result of changes in the absorption coefficients due to a shift in the band edge.

In order the determine the surface recombination velocity of the SiO_2–Si interface, it is also highly desirable to have spectral response measurements in the very high absorption regime of .35 - .4 μm. Accurate measurements of the internal quantum efficiencies are difficult to obtain at these wavelengths.

Effects of Band Gap Narrowing on Long Wave Length Absorption Coefficients

At the present time no corrections for the effect of band gap narrowing are made to the absorption coefficients.

Carrier-Carrier Scattering

Carrier-carrier scattering can be a significant effect in high concentration solar cells, and will become a significant effect in one sun solar cells as the efficiency is increased.

High Injection Lifetime

At the present time very little data is available on majority carrier lifetime. A typical modeling approach is to assume that the majority carrier lifetime is the same as minority carrier lifetime. This seems to give reasonably good agreement with cell performance under high injection conditions, but direct measurement of the high injection lifetime would be highly desirable.

Conclusions

One and two-dimensional device models have been quite successfully employed as an aid to design, interpretation, sensitivity analysis, and prediction. However, the predictive capability of any device code is only as good as the physics which is modeled and the data which is supplied. If further improvements are to be made in the performance of single crystal silicon solar cells, careful attention will have to be paid to both of these areas and a great deal of effort will have to be devoted to measurement techniques which will allow the independent determination of the parameters which must be supplied to the device code.

Acknowledgment

SCAP1D and SCAP2D were developed under the sponsorship of Sandia National Laboratories on contract number 52-5675.

References

1. M. S. Lundstrom, R. J. Schwartz, "Annual Report on Interdigitated Back Contact Solar Cells," TR-EE 80-14, School of Electrical Engineering, Purdue University, West Lafayette, IN.

2. R. J. Schwartz, M. S. Lundstrom, J. L. Gray, "Annual Report on High Intensity Solar Cells, TR-EE 82-5, School of Electrical Engineering, Purdue University, West Lafayette, IN.

3. R. J. Schwartz, J. L. Gray, M. S. Lundstrom, "Report on High Intensity Solar Cells," TR-EE 83-21, School of Electrical Engineering, Purdue University, West Lafayette, IN.